

A SUCCESSFUL BROAD-BAND SURVEY FOR GIANT Ly α NEBULAE I: SURVEY DESIGN AND CANDIDATE SELECTION

MOIRE K. M. PRESCOTT^{1,2}, ARJUN DEY³, BUELL T. JANNUZI³

Draft version November 15, 2018

ABSTRACT

Giant Ly α nebulae (or Ly α “blobs”) are likely sites of ongoing massive galaxy formation, but the rarity of these powerful sources has made it difficult to form a coherent picture of their properties, ionization mechanisms, and space density. Systematic narrow-band Ly α nebula surveys are ongoing, but the small redshift range covered and the observational expense limit the comoving volume that can be probed by even the largest of these surveys and pose a significant problem when searching for such rare sources. We have developed a systematic search technique designed to find large Ly α nebulae at $2 \lesssim z \lesssim 3$ within deep *broad-band* imaging and have carried out a survey of the 9.4 square degree NOAO Deep Wide-Field Survey (NDWFS) Boötes field. With a total survey comoving volume of $\approx 10^8 h_{70}^{-3} \text{ Mpc}^3$, this is the largest volume survey for Ly α nebulae ever undertaken. In this first paper in the series, we present the details of the survey design and a systematically-selected sample of 79 candidates, which includes one previously discovered Ly α nebula.

Subject headings: galaxies: formation — galaxies: evolution — galaxies: high-redshift — galaxies: surveys

1. INTRODUCTION

Giant radio-quiet Ly α nebulae (e.g., Francis et al. 1996; Steidel et al. 2000; Palunas et al. 2004; Matsuda et al. 2004; Dey et al. 2005; Saito et al. 2006; Nilsson et al. 2006; Smith & Jarvis 2007; Greve et al. 2007; Yang et al. 2009) likely provide an observational window into the physics of ongoing massive galaxy formation. As large as ~ 100 kpc across, Ly α nebulae emit copious Ly α emission ($\sim 10^{44} \text{ erg s}^{-1}$), signaling the presence of highly energetic phenomena. Ly α nebulae are sometimes surrounded by or associated with young, star-forming galaxy populations and obscured AGN (e.g., Chapman et al. 2001; Basu-Zych & Scharf 2004; Matsuda et al. 2004; Dey et al. 2005; Geach et al. 2007, 2009, Prescott et al. 2012c, submitted) and have been shown to reside in overdense environments (Matsuda et al. 2004, 2005, 2009; Saito et al. 2006; Prescott et al. 2008; Yang et al. 2009, 2010). Studying Ly α nebulae can provide important insight into the process of galaxy formation, but after a decade of study, we have not yet developed a complete understanding of the dominant power source or, even more fundamental, the space density of Ly α nebulae.

The problem lies in having such a small sample - only a few dozen large (~ 100 kpc) Ly α nebulae are currently known - and in attempting to measure the space density of a rare population over restricted volumes. Radio-quiet Ly α nebulae were first discovered in targeted narrow-band imaging studies of known overdensities (e.g., Francis et al. 1996; Steidel et al. 2000; Matsuda et al. 2004). Since then, the sample has slowly

grown as a result of ever more expensive narrow-band surveys over increasingly wide areas (e.g., Nilsson et al. 2006; Smith & Jarvis 2007; Saito et al. 2006; Yang et al. 2009, 2010; Matsuda et al. 2011). Building a sufficient sample of such rare objects over a wide range of environments and accurately measuring their space density requires surveying larger comoving volumes than are typically feasible via standard narrow-band imaging.

We have therefore taken a complementary approach by developing a systematic search algorithm to find luminous Ly α nebulae at $2 \lesssim z \lesssim 3$ using deep *broad-band* imaging and have tested the technique using archival imaging data from the NOAO Deep Wide-Field Survey (NDWFS; Jannuzi & Dey 1999). We describe our systematic broad-band Ly α nebula survey in three papers. This paper (Paper I) discusses the survey design and candidate selection approach. In Section 2, we describe the algorithm used to select Ly α nebulae. Section 3 presents the sample of 39 first priority and 40 second priority Ly α nebula candidates selected from archival imaging of the Boötes Field of NDWFS and discusses the potential sources of contamination. In Section 4, we address the complementarity of our approach relative to traditional narrow-band surveys, and we conclude in Section 5. Discussions of (a) our successful spectroscopic follow-up campaign and (b) the survey selection function and implied Ly α nebula number density are presented in the two subsequent papers in this series (Prescott et al. 2012b and Prescott et al. 2013, in preparation; hereafter, Paper II and III).

We assume the standard Λ CDM cosmology ($\Omega_M = 0.3$, $\Omega_\Lambda = 0.7$, $h = 0.7$); $1''$ corresponds to a physical scales of 8.5-7.6 kpc for redshifts of $z \approx 2 - 3$. All magnitudes are in the AB system.

2. SURVEY DESIGN

While most of the early examples of the Ly α nebula class were found via narrow-band surveys of known galaxy overdensities, one of the largest Ly α nebulae

¹ TABASGO Postdoctoral Fellow; Department of Physics, Broida Hall, Mail Code 9530, University of California, Santa Barbara, CA 93106, USA; mkpresco@physics.ucsb.edu

² Steward Observatory, University of Arizona, 933 N. Cherry Avenue, Tucson, AZ 85721, USA

³ National Optical Astronomy Observatory, 950 North Cherry Avenue, Tucson, AZ 85719, USA

was discovered in a very different manner (LABd05; Dey et al. 2005). This Ly α nebula at $z \approx 2.7$ came to light during a study of strong 24 μ m sources detected by the Spitzer Space Telescope in the NDWFS Boötes field. Strikingly, this source had a diffuse, extended morphology and very blue colors in deep broad-band imaging. The authors suspected and spectroscopically confirmed that Ly α line and blue continuum emission were dominating the broad-band flux and that the diffuse morphology indicated the presence of a giant, spatially extended Ly α nebula.

Inspired by this discovery, we developed a search for Ly α nebulae designed to work on deep broad-band imaging and applied it to the ≈ 9 square degree NDWFS Boötes field dataset. Using a deep, wide-area, ground-based imaging survey like NDWFS allows us to probe an enormous comoving volume with existing data and significantly reduce the amount of new telescope time required to complete the program. In that sense, our survey is complementary to the more sensitive but smaller volume narrow-band Ly α nebulae surveys (e.g., Matsuda et al. 2004; Saito et al. 2006; Smith & Jarvis 2007; Yang et al. 2009, 2010; Matsuda et al. 2011). In this section we describe the NDWFS dataset and introduce the search algorithm used to select a sample of Ly α nebulae candidates.

2.1. NDWFS Broad-band Data

Our survey technique was built and tested using the broad-band optical imaging from NDWFS, data which are available through the NOAO Science Archive.⁴ The B_W and R -band images of the 9.4 square degree Boötes field were obtained using the Mayall 4m Telescope and the MOSAIC 1 prime focus camera. The Boötes field was originally selected as a field suitable for a deep extragalactic survey because of its low 100 μ m background and N(HI) column density along the line of sight, and for being well positioned from Kitt Peak National Observatory during a period of the year with historically good observing conditions. The entire Boötes field was covered using stacked observations of 27 overlapping MOSAIC pointings. The resulting median seeing was 1.10'' and 1.10'' in the B_W and R bands, respectively, and the median point-source depths were ≈ 26.3 and 25.2 AB mag (5σ ; 2'' diameter apertures). The median 1σ B_W surface brightness limit is 28.9 mag arcsec⁻² (1.1'' diameter apertures), which corresponds (in the case of pure line emission) to a line flux surface brightness limit of 2.48×10^{-17} erg s⁻¹ cm⁻² arcsec⁻². The data were reduced by the NDWFS team using IRAF⁵.

2.2. The Search Algorithm

The goal of our systematic survey was to find large, luminous Ly α nebulae similar to LABd05. The search pipeline uses a blue broad-band image — in the case of the NDWFS, the B_W -band — as the primary search image and is tuned to find diffuse, spatially extended, low surface brightness objects. It is most sensitive to extended sources for which a bright Ly α emission line boosts the broad-band flux relative to the very dark sky in the blue (Figure 1), i.e., the largest and brightest Ly α

nebulae. A redder band — the R -band in the case of NDWFS — is used to derive secondary color information.

Given the depth and the size of the imaging survey, in designing our search algorithm it was important to minimize the number of contaminant objects while retaining objects likely to be Ly α nebulae. Our search strategy therefore involved first subtracting off bright galaxies and compact objects and then using a wavelet deconvolution algorithm to select diffuse, spatially extended, low surface brightness objects with blue colors. The search pipeline steps are described in detail below and illustrated using a flowchart⁶ in Figure 2. Figures 3 and 4 show the pipeline at work on the image region near LABd05.

2.2.1. Background and Halo Subtraction

Step 1: The first step is to remove the sky background using a background map generated by Source Extractor (Version 2.4.4; Bertin & Arnouts 1996). We used a high detection threshold (DETECT_THRESH = 10σ per pixel), set background parameters (BACK_SIZE = 64 and BACK_FILTERSIZE = 3), and required a minimum of 5 connected pixels (DETECT_MINAREA = 5). This background map, which includes a contribution from the halos around bright stars, was subtracted from the search image.

2.2.2. Bright Object Removal

In order to remove bright stars and galaxies that may contaminate the final candidate list, we employed the following procedure.

Step 2: We first ran Source Extractor with a high detection threshold (DETECT_THRESH = 10σ per pixel) and a minimum of 5 connected pixels (DETECT_MINAREA = 5) in order to generate a catalog of bright sources.

Step 3: We then ran Source Extractor with a very low threshold (DETECT_THRESH = 1σ per pixel) in order to generate a deep segmentation map, i.e., a map of all object pixels, that would include pixels in the faint wings of bright stars and galaxies. This iteration used the ASSOC mode in which the catalog from *Step 2* was used as an input to Source Extractor and only those detections that match were included in the catalog. Detected sources were matched against the input catalog in a weighted fashion based on measured pixel position (X_IMAGE, Y_IMAGE), the object flux (FLUX_AUTO), and a search radius (ASSOC_RADIUS = 2 pixels). Using the deep segmentation maps from this step and the image rms maps, we replaced regions identified with bright stars and galaxies with patches of sky noise.

Step 4: We ran Source Extractor on the “cleaned” image from *Step 3* but this time with an intermediate threshold (DETECT_THRESH = 6σ per pixel, determined based on visual inspection) to further remove stars and galaxies.

Step 5: We ran Source Extractor on the image from *Step 4* with the ASSOC feature in order to generate the corresponding deep segmentation map. Again, the detections are replaced with sky noise.

2.2.3. Faint Compact Object Removal

⁴ NOAO Science Archive: <http://archive.noao.edu/nsa/>

⁵ NDWFS Data Processing: <http://www.noao.edu/noao/noaodeep/>

⁶ Flowchart created using Omnigraffle: <http://www.omnigroup.com/products/omnigraffle/>

Step 6: We next used unsharp masking to remove fainter objects with compact morphology. An unsharp masked image was produced by smoothing the image from *Step 5* using an 11×11 pixel kernel and then subtracting the smoothed image from the original *Step 5* image. In this process, diffuse emission was removed, leaving only compact sources in the unsharp masked image.

Step 7: We performed another ASSOC Source Extractor run on the unsharp masked image in which we only allowed matched detections to be included in the catalog, i.e., anything detected in both the *Step 5* image and the unsharp masked image was reported. We removed these object regions by replacing them with sky noise, and in this way removed additional faint compact sources from the image.

2.2.4. Final Image Cleaning

Step 8: To avoid artifacts (e.g., saturated columns, poorly-subtracted halos) from bright stars being selected as sources later in the pipeline, we replaced the regions around bright stars ($B < 16$ mag in the USNO-A2.0 catalog) out to a radius of 150 pixels ($\approx 39''$) with sky noise. This step removed ≈ 0.68 square degrees from the final survey area.

2.2.5. Identification of Spatially Extended Objects

Step 9: We then applied a wavelet decomposition algorithm to decompose the image into maps showing the power on a number of different spatial scales.

The basic idea behind wavelet decomposition is to decompose the image into a set of “wavelet planes,” each of which contains the flux of sources with power on that scale and the sum of which is the original image (ignoring losses). The power of the wavelet decomposition approach is to reduce the interference of small scale objects when looking for large scale structures.

We use the wavelet decomposition code *wvdecomp*⁷ to filter the image across six size scales ($scale_{min} = 1$, $scale_{max} = 6$, $threshold = 3$, $threshold_{min} = 2$, $iter = 10$). Here we give a brief description of the algorithm; a detailed discussion of the code is given in the ZHTOOLS documentation. The *wvdecomp* algorithm uses an *à trous* wavelet kernel which is defined as the difference between two functions (f_i and f_{i+1}) that each roughly resemble a Gaussian of width 2^{i-1} . On each scale, the kernel is sensitive to objects of the same size ($\approx 2^{i-1}$).

The algorithm begins by convolving the image with the smallest wavelet kernel. Any features that are insignificant in the convolved image are zeroed and the result is subtracted from the original image, causing a majority of the flux from small features comparable in size to the smallest wavelet kernel to be removed. The process is repeated with larger and larger wavelet kernels, and the results from each step are saved as wavelet power maps or “wavelet planes.” To minimize the loss of information at each step, two thresholds are specified in running the code: a detection threshold, t_{max} , and a filtering threshold, t_{min} , both defined in terms of the image noise. A

source detected on a given scale above t_{min} is counted as significant only if the source local maximum also exceeds t_{max} .

Step 10: We used the known Ly α nebula LABd05 to empirically determine the appropriate scale for large Ly α nebulae. Using one final run of SourceExtractor, we generate a catalog of sources in the wavelet power map and select those with wavelet power peaks above 4σ , chosen to minimize the number of total candidates while preserving sources like LABd05.

2.2.6. Final Catalog Cleaning and Candidate Prioritization

Step 11: Sources drawn from low exposure time regions of the survey (< 4000 sec) as well as those found in regions that had been flagged in previous steps were removed from the candidate list. This step removed ≈ 0.28 square degrees from the final survey area.

Step 12: Postage stamps of candidates were inspected visually and classified by eye using morphological flags, where STAR denotes a star halo, GALAXY denotes a galaxy halo, TIDAL/ARM indicates tidal tails or spiral arms, GROUP corresponds to a tight grouping of compact sources selected as a single large source, and DIFFUSE indicates spatially extended diffuse emission. The 2266 sources selected by the morphological search pipeline were categorized as follows: 738 STAR sources, 491 GALAXY sources, 170 TIDAL/ARM sources, 459 GROUP sources, and 408 DIFFUSE sources. We removed those objects categorized as STAR, GALAXY, and TIDAL/ARM from the candidate sample (1399 sources), since these are easy to classify unambiguously by eye. As the distinction between categories GROUP and DIFFUSE is more subjective, both category GROUP and DIFFUSE objects were included in the final sample (867 sources).

2.2.7. Candidate Selection

Step 13: The final sample was then prioritized based on $B_W - R$ color and size, giving priority to blue candidates with large sizes. Figure 5 shows the size and color distribution of the candidate sample. We measured $B_W - R$ colors in the original images using large apertures (30 pixel, $7.7''$ diameter, i.e., roughly 60 kpc; aperture sky subtraction). The size of each source, for the purposes of selecting candidates, was taken to be the size measured in the wavelet power map (ISOAREA_WORLD in square degrees), as determined by SourceExtractor during the final search (*Step 10*). While representative, this “wavelet size” should not be taken to be the true size of the object. The wavelet size typically underestimates the nebular extent in cases where some portion of that object has been rejected during the pipeline (due to compact sources within or adjacent to the diffuse emission). In addition, as we are attempting to detect line emission within the broad B_W band, the measured B_W sizes will underestimate the true nebular size. We investigate this in more detail in Paper II.

The majority of the morphologically-selected candidates are red ($B_W - R \gtrsim 0.5$), but a small subset show blue colors, which could either result from a strong emission line within the B_W band (Ly α at $1.9 < z < 2.9$), from very blue continuum emission, or a combination. Figure 6 shows the expected $B_W - R$ color for a model source with a given redshift and Ly α equivalent width generated by adding a Gaussian emission line to a flat

⁷ *wvdecomp* was written by Alexey Vikhlinin; ZHTOOLS documentation and source code: <http://hea-www.harvard.edu/RD/zhtools/>.

spectrum source ($f_\lambda \propto \lambda^{-2}$). Unlike narrow-band Ly α nebula surveys, our survey is not formally equivalent width limited. Other than at the high redshift end of the survey ($z \gtrsim 2.7$), sources of any equivalent width will fall within our color selection window as long as they are spatially extended enough and bright enough in B_W to be selected via the morphological search pipeline. However, given the distribution of field galaxy colors we expect that sources with bluer colors are more likely to be Ly α nebulae. Given the number of candidates we expected to be able to target during our spectroscopic follow-up campaign, we therefore defined our first priority region as $B_W - R < 0.45$ and $\text{ISOAREA_WORLD} > 34 \text{ arcsec}^2$ and a second priority region as $0.45 < B_W - R < 0.65$ and $\text{Log}(\text{ISOAREA_WORLD}) > 0.934 \times (B_W - R) + 1.11 \text{ arcsec}^2$ (Figure 5). Our spectroscopic follow-up observations (using the MMT/Blue Channel Spectrograph with a full wavelength range of $\Delta\lambda = 3100\text{--}8320\text{\AA}$) are able to detect line emission from Ly α nebulae down to $z \approx 1.6$, leading to a total survey redshift range of $1.6 < z < 2.9$. The details of our selection function will be treated in Paper III.

3. CANDIDATE SAMPLE

Our final candidate sample consists of 39 first priority and 40 second priority sources over a search area of 8.5 square degrees (Table 1). Of the 39 first priority sources, 32 have a morphological category of GROUP and 7 are in the category DIFFUSE; for the 40 second priority sources, 31 are in the GROUP category and 9 in the DIFFUSE category. The distribution of Ly α nebulae candidates on the sky is shown in Figure 7, and postage stamps of the B_W , R , and I -band imaging of all candidates are shown in Appendix A. Due to the fact that we included both category GROUP and DIFFUSE sources in the final catalog, the candidates span a range of morphologies from clumpy to diffuse. In particular, a number of the very blue sources appear to be a close grouping of compact sources selected as one. While at first glance these compact groups do not have the diffuse appearance we expect for Ly α nebulae, it could be unwise to remove them because the full morphological range spanned by the Ly α nebula class is not well-known and some Ly α nebulae are known to include compact sources (e.g., young galaxies; Prescott et al. 2012c, submitted). For these reasons we did not apply any further morphological selection criteria to the main sample. In addition to our 79 systematically-selected first and second priority samples, we also flagged 6 additional candidates with promising morphologies from outside these regions as a test of our color-selection approach. Of the third priority sources, which are included for reference in Table 1 and Appendix A, 5 have a morphological category of DIFFUSE and 1 is in the category GROUP.

Based on previous narrow-band Ly α nebulae surveys, we can predict the number of Ly α nebulae we would expect to find within our full survey volume. Figure 8 shows the cumulative number of Ly α nebulae expected assuming a constant comoving volume density as a function of redshift of $0.5 \times 10^{-6} - 3.6 \times 10^{-6} \text{ Mpc}^{-3}$ (the range spanned by the estimates of Yang et al. 2009) and a 100% detection success rate. This non-evolving model would predict approximately 60-400 Ly α nebulae over the redshift range of our survey ($1.6 \lesssim z \lesssim 2.9$). As the comoving volume density of Ly α nebulae is unlikely

to remain constant over cosmic time (Keel et al. 2009), for comparison we also plot the cumulative number of Ly α nebulae expected within our survey area assuming that the comoving volume density increases linearly as a function of redshift (dashed lines). In reality the selection function, completeness, and efficiency of our survey are different from that of narrow-band surveys such as Yang et al. (2009) and the evolution of the Ly α nebula comoving volume density is unknown; we address these issues in more detail in Paper III.

3.1. Potential Contaminants

Due to the wide bandpass of the B_W filter, there are several populations that may contaminate our Ly α nebula candidate sample. The morphological selection method will tend to pick out any source of low surface brightness extended emission that cannot be easily identified, e.g., a low surface brightness galaxy (LSB) or low surface brightness nebulae within the Galaxy. In principle, lower redshift sources with [OII] $\lambda\lambda 3727, 3729$ emission in the selection band (B_W) are a contaminant population, much as they are in Ly α -emitting galaxy surveys. In addition, galaxies and Ly α nebulae in the redshift desert (i.e., $1.2 < z < 1.6$) may be selected as candidates in our survey if they exhibit extended blue continuum emission or a close grouping of compact sources. In these cases, Ly α would be positioned blueward and [OII] redward of the wavelength range of our follow-up spectroscopy, leading us to detect faint, spatially extended, blue continuum emission with no emission lines to provide confirmation of the redshift.

While this range of different populations could contaminate our sample in principle, not all of them will contribute substantially in practice. We do not expect to find many LSBs because the $B_W - R$ colors of Ly α nebulae are likely to be bluer than typical LSB colors (i.e., $B_W - R = 1.49 \pm 0.60$; Habertz et al. 2007); any blue LSBs would be expected to show optical emission lines and therefore easily identified in follow-up spectroscopy. If compact groupings of [OII]-emitters or extended [OII] nebulae were to be selected via our morphological search, the position of [OII] in the B_W , [OIII] in the R band, and H α in the R or I band would give the object redder colors, which would not be included in the final sample. On the other hand, a primary contaminant population will be galaxies or Ly α nebulae in the redshift range $1.2 \lesssim z \lesssim 1.6$ that appear in optical spectroscopy as spatially extended continuum-only sources. From Figure 8, we would expect of order 20-180 such sources, or roughly 25% of the predicted Ly α nebulae sample over the entire redshift range ($1.2 \lesssim z \lesssim 2.9$), assuming no evolution in the intrinsic number density. With line emission outside the optical window, however, follow-up observations with HST will be necessary to confirm whether or not any continuum-only sources are in fact lower redshift Ly α nebulae.

4. DISCUSSION

4.1. A Successful Broad-band Ly α Nebula Survey

Our systematic broad-band Ly α nebula search was designed to find luminous Ly α nebulae similar to LABd05. Subsequent spectroscopic follow-up of a subset of our morphological candidate sample showed that, in addition to recovering the previously-discovered large Ly α

nebula at $z \approx 2.66$ (LABd05; Dey et al. 2005), this novel approach was able to successfully locate 4 new large Ly α nebulae over the NDWFS Boötes field at $z \approx 1.67$, $z \approx 2.27$, $z \approx 2.14$, and $z \approx 1.88$ (PRG1, PRG2, PRG3, PRG4; Prescott 2009). Of particular note, our broad-band search identified the first spatially extended Ly α +HeII nebula (PRG1; Prescott et al. 2009); located at $z \approx 1.67$, this system is the lowest redshift Ly α nebula known, and the strong HeII emission suggests that it may contain low metallicity gas. The 5 confirmed Ly α nebulae are shown for reference in Figures 5-6, 7, and 9. A full discussion of the spectroscopic follow-up campaign is presented in Paper II, and the selection function and implied space density for this survey are discussed in Paper III.

4.2. Comparisons to Other Surveys

While broad-band imaging has been used in recent years to isolate samples of Ly α -emitting and Ly α -absorbing galaxies based on colors (Cooke 2009) and to find strong line-emitting nebulae at low redshifts through the Galaxy Zoo project (Lintott et al. 2009; Keel et al. 2011), our search is the first time broad-band data has been used as the basis for a semi-automated systematic morphological survey for high redshift Ly α nebulae. Our Ly α nebula survey is also fundamentally different and complementary to standard narrow-band surveys for Ly α nebulae (Table 2). The pilot survey of the NDWFS Boötes field has shown that it is possible to find large Ly α nebulae using deep broad-band imaging data. There are many advantages to this unusual approach. A broad-band search is able to efficiently cover enormous comoving volumes that would be observationally expensive when using a narrow-band filter. A narrow-band survey using a 100Å filter at $z \approx 2.3$ would need to search over 100 square degrees to reach the same comoving volume covered in our broad-band survey of the NDWFS Boötes field ($\approx 10^8 h_{70}^3 \text{ Mpc}^{-3}$). In addition, our technique builds on existing datasets, which means that our search algorithm can be easily modified to find Ly α nebulae within any deep, broad-band, wide-field imaging survey, leading to substantially lower observational overhead. Finally, while the early, successful Ly α surveys often targeted known overdensities and were limited to smaller areas (Steidel et al. 2000; Matsuda et al. 2004; Francis et al. 1996; Palunas et al. 2004), introducing a bias to the number density estimates, our 8.5 square degree survey, by contrast, is unbiased in terms of environment, spanning a $\Delta z \approx 1.3$, a comoving transverse distance of $\approx 290 h_{70}^{-1} \text{ Mpc}$ (at the redshift midpoint, $z \approx 2.25$), and a comoving line-of-sight distance of $\approx 1700 h_{70}^{-1} \text{ Mpc}$.

At the same time, a drawback of using broad-band data to select line-emitting sources is the necessity of restricting our search to the largest, most luminous Ly α nebulae and of removing compact sources in favor of diffuse emission, in order to reduce the number of contaminants. Thus, while our search successfully recovered a sample of Ly α nebulae, a handful of other (fainter or more compact) Ly α nebulae that were identified by traditional narrow-band searches in Boötes were not recovered by our broad-band search (Table 3).

In Figure 9, we show the B_W isophotal area and mean

surface brightness estimates for the candidate sample, as derived using SourceExtractor (DETECT_THRESH= 28.9 mag arcsec $^{-2}$, DETECT_MINAREA= 5) on the original B_W imaging, for the Ly α nebulae confirmed by our survey (Paper II), and for other known Ly α nebula sources in the field. The sources our survey did not recover fall into two categories: either the Ly α emission surrounds a much brighter compact continuum source (“core-halo” morphology) or the diffuse B_W emission is simply too faint to be selected by our search algorithm. In the first category are the four Ly α nebulae found by Yang et al. (2009) using a traditional narrow-band survey of NDWFS Boötes; all four consist of bright continuum sources (AGN in two cases) surrounded by Ly α halos that are undetected in the broad-band B_W imaging. The bright compact central sources caused these objects to be rejected and replaced with sky noise during Steps 2-3 or Steps 6-7 of the search pipeline. Intermediate-band imaging with the Subaru (Prescott et al. 2008) and Mayall Telescopes revealed three additional Ly α nebulae that were not detected using the broad-band search algorithm. One case (P1) was too faint to be selected by our search algorithm, and two other cases (P2 & P3) showed core-halo morphologies with confirmed Ly α emission (at $z \approx 2.6$ and $z \approx 1.9$) in the midst of several bright continuum sources. With the compact sources removed by the search pipeline, the wings of the Ly α emission were still detected in the B_W imaging in each case, but at weaker wavelet power limits than probed by the current survey.

As our search was designed to select large, luminous, and diffuse Ly α nebulae, it is not surprising that more compact or fainter Ly α nebulae were not selected. In future work, it will be important to understand this range of Ly α nebula morphologies and whether they reflect fundamentally different sources or simply different evolutionary phases of the same underlying phenomenon.

5. CONCLUSIONS

We have designed an innovative systematic search for large Ly α nebulae using deep broad-band data. Our technique is designed to find the largest and brightest Ly α nebulae and is able to probe enormous comoving volumes ($\approx 10^8 h_{70}^{-3} \text{ Mpc}^3$) using existing deep broad-band datasets. In this paper, we presented details on the survey design and our sample of Ly α nebula candidates selected from the NDWFS Boötes Field. Paper II of this series presents the spectroscopic follow-up and the confirmed Ly α nebula sample, and Paper III will address the details of the survey selection function and the implications for the space density of Ly α nebulae. In the future, we will build on the search algorithm developed in this work in order to find Ly α nebulae in other deep and wide imaging fields and increase the sample of known Ly α nebulae available for detailed follow-up study.

The authors are grateful to Alexey Vikhlinin for the use of the code *wdecamp*. This research draws upon data from the NDWFS as distributed by the NOAO Science Archive. NOAO is operated by the Association of Universities for Research in Astronomy (AURA), Inc. under a cooperative agreement with the National Science Foundation. M. P. was supported by a NSF Graduate Research Fellowship and a TABASGO Prize Postdoctoral

Fellowship. A. D. and B. T. J.'s research is supported by NOAO, which is operated by AURA under a cooperative agreement with the National Science Foundation.

REFERENCES

- Basu-Zych, A., & Scharf, C. 2004, *The Astrophysical Journal*, 615, L85
- Bertin, E., & Arnouts, S. 1996, *Astronomy and Astrophysics Supplement*
- Chapman, S. C., Lewis, G. F., Scott, D., Richards, E., Borys, C., Steidel, C. C., Adelberger, K. L., & Shapley, A. E. 2001, *The Astrophysical Journal*, 548, L17
- Charlot, S., & Fall, S. M. 1993, *The Astrophysical Journal*, 415, 580
- Cooke, J. 2009, *The Astrophysical Journal*, 704, L62
- Dey, A., et al. 2005, *The Astrophysical Journal*, 629, 654
- Francis, P. J., et al. 1996, *The Astrophysical Journal*, 457, 490
- Geach, J. E., Smail, I., Chapman, S. C., Alexander, D. M., Blain, A. W., Stott, J. P., & Ivison, R. J. 2007, *The Astrophysical Journal*, 655, L9
- Geach, J. E., et al. 2009, *The Astrophysical Journal*, 700, 1
- Greve, T. R., Stern, D., Ivison, R. J., De Breuck, C., Kovács, A., & Bertoldi, F. 2007, *Monthly Notices of the Royal Astronomical Society*, 382, 48
- Haberzettl, L., Bomans, D. J., Dettmar, R.-J., & Pohlen, M. 2007, *Astronomy and Astrophysics*, 465, 95
- Jannuzi, B. T., & Dey, A. 1999, in *Photometric Redshifts and the Detection of High Redshift Galaxies*, ed. R. Weymann, R., Storrie-Lombardi, L., Sawicki, M., & Brunner, Vol. 191 (Astronomical Society of the Pacific Conference Series), 111
- Keel, W. C., White, R. E., Chapman, S., & Windhorst, R. A. 2009, *The Astrophysical Journal*, 138, 986
- Keel, W. C., et al. 2011, *Monthly Notices of the Royal Astronomical Society*, 420, 878
- Lilly, S. J., Cowie, L. L., & Gardner, J. P. 1991, *The Astrophysical Journal*, 369, 79
- Lintott, C. J., et al. 2009, *Monthly Notices of the Royal Astronomical Society*, 399, 129
- Matsuda, Y., et al. 2004, *The Astrophysical Journal*, 128, 569
- Matsuda, Y., et al. 2005, *The Astrophysical Journal*, 634, L125
- Matsuda, Y., et al. 2009, *Monthly Notices of the Royal Astronomical Society: Letters*, 400, L66
- Matsuda, Y., et al. 2011, *Monthly Notices of the Royal Astronomical Society: Letters*, 410, L13
- Nilsson, K. K., Fynbo, J. P. U., Møller, P., Sommer-Larsen, J., & Ledoux, C. 2006, *Astronomy and Astrophysics*, 452, L23
- Ouchi, M., et al. 2009, *The Astrophysical Journal*, 696, 1164
- Palunas, P., Teplitz, H. I., Francis, P. J., Williger, G. M., & Woodgate, B. E. 2004, *The Astrophysical Journal*, 602, 545
- Prescott, M. K. M. 2009, Phd, University of Arizona
- Prescott, M. K. M., Dey, A., & Jannuzi, B. T. 2009, *The Astrophysical Journal*, 702, 554
- Prescott, M. K. M., Kashikawa, N., Dey, A., & Matsuda, Y. 2008, *The Astrophysical Journal*, 678, L77
- Saito, T., Shimasaku, K., Okamura, S., Ouchi, M., Akiyama, M., & Yoshida, M. 2006, *The Astrophysical Journal*, 648, 54
- Smith, D. J. B., & Jarvis, M. J. 2007, *Monthly Notices of the Royal Astronomical Society: Letters*, 378, L49
- Steidel, C. C., Adelberger, K. L., Shapley, A. E., Pettini, M., Dickinson, M., & Giavalisco, M. 2000, *The Astrophysical Journal*, 532, 170
- Yang, Y., Zabludoff, A., Eisenstein, D., & Davé, R. 2010, *The Astrophysical Journal*, 719, 1654
- Yang, Y., Zabludoff, A., Tremonti, C., Eisenstein, D., & Davé, R. 2009, *The Astrophysical Journal*, 693, 1579

Table 1
Ly α Nebula Candidates

Candidate Name	Right Ascension (J2000 hrs)	Declination (J2000 deg)	Wavelet Size (arcsec ²)	Morphological Flag ^a	B_W^b (AB mag)	$B_W - R^b$ (AB mag)	Priority ^c	
1)	NDWFS J143004.7+353509	14:30:04.687	35:35:09.06	134.0	DIFFUSE	23.79±0.05	0.61	2 ^d
2)	NDWFS J143006.9+353437	14:30:06.864	35:34:36.73	108.2	DIFFUSE	23.05±0.03	0.80	3 ^d
3)	NDWFS J142846.2+330819	14:28:46.228	33:08:19.42	89.9	DIFFUSE	23.00±0.03	0.89	3
4)	NDWFS J143436.4+330406	14:34:36.448	33:04:05.62	72.1	GROUP	22.90±0.02	0.53	2
5)	NDWFS J142855.0+353022	14:28:54.998	35:30:21.70	64.9	DIFFUSE	23.26±0.03	0.52	2
6)	NDWFS J143153.1+351436	14:31:53.066	35:14:36.45	62.6	GROUP	23.31±0.04	0.53	2
7)	NDWFS J143055.2+352855	14:30:55.192	35:28:54.76	61.6	GROUP	23.30±0.04	0.43	1
8)	NDWFS J143057.7+354547	14:30:57.662	35:45:47.26	59.6	GROUP	23.09±0.03	0.43	1
9)	NDWFS J143842.0+335325	14:38:41.956	33:53:24.79	59.5	GROUP	23.14±0.04	0.63	2
10)	NDWFS J143410.9+331731	14:34:10.948	33:17:30.80	59.1	DIFFUSE	23.18±0.03	0.42	1 ^e
11)	NDWFS J142729.9+341125	14:27:29.894	34:11:25.22	56.2	GROUP	23.48±0.05	0.48	2
12)	NDWFS J143551.3+333421	14:35:51.278	33:34:21.03	55.9	GROUP	23.38±0.05	0.51	2
13)	NDWFS J142909.3+342542	14:29:09.278	34:25:42.38	55.8	GROUP	23.41±0.04	0.58	2
14)	NDWFS J143512.3+351109	14:35:12.336	35:11:08.62	55.7	DIFFUSE	23.53±0.04	0.56	2 ^f
15)	NDWFS J142906.3+341130	14:29:06.271	34:11:30.26	53.5	GROUP	23.47±0.04	0.48	2
16)	NDWFS J142856.0+331937	14:28:56.013	33:19:36.51	53.5	GROUP	23.38±0.04	0.60	2
17)	NDWFS J143511.0+335543	14:35:11.030	33:55:43.10	53.3	GROUP	23.12±0.03	0.53	2
18)	NDWFS J143222.8+324943	14:32:22.768	32:49:42.67	53.1	DIFFUSE	23.35±0.04	0.53	2
19)	NDWFS J143302.8+354729	14:33:02.844	35:47:29.43	52.7	GROUP	23.42±0.04	0.50	2
20)	NDWFS J143641.4+341510	14:36:41.373	34:15:10.26	52.1	GROUP	23.50±0.04	0.55	2
21)	NDWFS J143230.2+334105	14:32:30.244	33:41:05.46	50.5	GROUP	23.25±0.03	0.56	2
22)	NDWFS J142819.8+344657	14:28:19.840	34:46:57.14	50.4	GROUP	23.16±0.03	0.61	2
23)	NDWFS J143115.1+354148	14:31:15.055	35:41:47.76	50.1	GROUP	23.54±0.05	0.55	2
24)	NDWFS J142614.7+344434	14:26:14.714	34:44:34.22	49.9	GROUP	23.51±0.05	0.43	1
25)	NDWFS J142929.2+354711	14:29:29.198	35:47:10.78	49.5	GROUP	23.17±0.03	0.52	2
26)	NDWFS J142622.9+351422	14:26:22.905	35:14:22.02	49.5	DIFFUSE	23.20±0.04	-0.49	1 ^g
27)	NDWFS J143055.7+340502	14:30:55.713	34:05:01.71	49.3	DIFFUSE	23.04±0.03	0.57	2
28)	NDWFS J143236.9+351800	14:32:36.883	35:18:00.32	49.1	GROUP	23.42±0.06	0.57	2
29)	NDWFS J142526.3+335112	14:25:26.332	33:51:12.16	48.7	GROUP	23.35±0.04	0.40	1
30)	NDWFS J143407.5+334141	14:34:07.476	33:41:40.56	48.3	GROUP	23.43±0.05	0.26	1
31)	NDWFS J142547.1+334454	14:25:47.126	33:44:54.13	48.1	DIFFUSE	22.98±0.03	0.45	1
32)	NDWFS J143459.7+333749	14:34:59.702	33:37:48.93	48.1	GROUP	23.68±0.06	0.48	2
33)	NDWFS J142714.8+343155	14:27:14.791	34:31:54.55	47.7	GROUP	23.38±0.04	0.52	2
34)	NDWFS J143128.2+352658	14:31:28.245	35:26:57.91	47.3	DIFFUSE	23.06±0.03	0.56	2
35)	NDWFS J142906.4+352432	14:29:06.398	35:24:32.22	47.2	GROUP	23.50±0.05	0.54	2

Table 1 — *Continued*

	Candidate Name	Right Ascension (J2000 hrs)	Declination (J2000 deg)	Wavelet Size (arcsec ²)	Morphological Flag ^a	B_W^b (AB mag)	$B_W - R^b$ (AB mag)	Priority ^c
36)	NDWFS J143422.3+351534	14:34:22.348	35:15:34.27	46.3	GROUP	23.50±0.04	0.51	2
37)	NDWFS J143310.3+335057	14:33:10.346	33:50:56.94	45.9	GROUP	23.82±0.07	0.58	2
38)	NDWFS J143523.9+354934	14:35:23.856	35:49:34.39	45.0	GROUP	23.93±0.07	0.42	1
39)	NDWFS J143053.5+352007	14:30:53.488	35:20:06.68	45.0	GROUP	23.02±0.04	0.43	1
40)	NDWFS J142653.2+343855	14:26:53.172	34:38:55.39	44.8	GROUP	23.53±0.06	-0.67	1 ⁱ
41)	NDWFS J142758.6+354428	14:27:58.617	35:44:28.42	44.4	GROUP	23.42±0.03	0.50	2
42)	NDWFS J142634.1+334954	14:26:34.106	33:49:53.61	44.3	GROUP	23.54±0.04	0.51	2
43)	NDWFS J143435.9+350710	14:34:35.932	35:07:09.91	44.2	GROUP	23.72±0.05	0.57	2
44)	NDWFS J142927.8+345906	14:29:27.837	34:59:06.14	43.1	GROUP	23.18±0.03	1.18	3
45)	NDWFS J142745.2+352949	14:27:45.194	35:29:48.98	42.9	GROUP	23.48±0.04	0.23	1
46)	NDWFS J142826.0+352116	14:28:25.999	35:21:15.62	42.7	GROUP	23.58±0.04	0.48	2
47)	NDWFS J142535.2+324934	14:25:35.205	32:49:34.17	42.6	GROUP	23.54±0.05	0.49	2
48)	NDWFS J142960.0+353927	14:29:59.978	35:39:26.89	42.4	GROUP	23.36±0.03	0.47	2
49)	NDWFS J142821.3+352001	14:28:21.259	35:20:00.92	42.4	GROUP	23.42±0.04	0.25	1
50)	NDWFS J143401.0+351229	14:34:01.034	35:12:29.12	42.0	GROUP	23.91±0.06	0.19	1
51)	NDWFS J143348.9+354157	14:33:48.885	35:41:56.68	41.7	GROUP	23.74±0.05	-0.08	1
52)	NDWFS J143706.6+335653	14:37:06.588	33:56:52.65	41.3	DIFFUSE	23.22±0.03	0.52	2
53)	NDWFS J142446.0+354714	14:24:45.998	35:47:14.06	40.5	GROUP	23.68±0.05	0.19	1
54)	NDWFS J142522.3+325424	14:25:22.339	32:54:23.65	39.9	GROUP	23.40±0.04	0.48	2
55)	NDWFS J143833.2+340359	14:38:33.249	34:03:59.32	39.6	GROUP	23.74±0.06	0.52	2
56)	NDWFS J143141.3+352110	14:31:41.253	35:21:09.86	39.5	DIFFUSE	23.17±0.05	0.48	2
57)	NDWFS J143416.4+333058	14:34:16.420	33:30:58.10	39.3	GROUP	23.26±0.05	0.46	2
58)	NDWFS J142516.6+324335	14:25:16.629	32:43:35.47	39.0	GROUP	23.13±0.04	0.14	1
59)	NDWFS J143412.7+332939	14:34:12.722	33:29:39.19	38.7	DIFFUSE	23.40±0.07	0.22	1 ^h
60)	NDWFS J142441.9+332532	14:24:41.940	33:25:31.94	38.4	GROUP	23.52±0.04	0.38	1
61)	NDWFS J143438.7+350420	14:34:38.700	35:04:19.84	38.4	DIFFUSE	23.72±0.05	0.46	2
62)	NDWFS J142832.7+354105	14:28:32.733	35:41:04.56	37.8	GROUP	23.72±0.05	-0.23	1
63)	NDWFS J143335.8+344503	14:33:35.764	34:45:02.84	37.5	GROUP	23.92±0.06	0.33	1
64)	NDWFS J143203.8+351855	14:32:03.760	35:18:54.86	37.4	GROUP	23.46±0.05	0.46	2
65)	NDWFS J143207.2+343101	14:32:07.224	34:31:01.34	37.3	DIFFUSE	23.30±0.03	0.81	3
66)	NDWFS J142539.9+344959	14:25:39.859	34:49:59.19	37.1	GROUP	23.57±0.04	0.14	1
67)	NDWFS J142819.7+325449	14:28:19.735	32:54:48.70	37.1	GROUP	23.44±0.03	0.44	1
68)	NDWFS J142443.9+344834	14:24:43.869	34:48:34.45	36.9	GROUP	23.64±0.05	0.37	1
69)	NDWFS J143202.6+351904	14:32:02.568	35:19:04.22	36.6	DIFFUSE	22.99±0.04	0.42	1
70)	NDWFS J142753.8+341204	14:27:53.762	34:12:04.10	36.5	DIFFUSE	23.29±0.04	0.45	1
71)	NDWFS J142600.8+350252	14:26:00.842	35:02:52.36	36.1	DIFFUSE	23.87±0.06	0.63	3
72)	NDWFS J142643.9+340937	14:26:43.850	34:09:36.82	36.1	GROUP	23.40±0.03	0.03	1
73)	NDWFS J142722.4+345225	14:27:22.408	34:52:24.74	35.9	GROUP	23.71±0.05	0.29	1
74)	NDWFS J142620.0+340427	14:26:19.982	34:04:27.01	35.7	GROUP	23.51±0.04	-0.75	1
75)	NDWFS J142707.8+344749	14:27:07.840	34:47:48.84	35.4	DIFFUSE	23.51±0.05	0.43	1
76)	NDWFS J142710.4+324842	14:27:10.447	32:48:41.76	35.4	GROUP	23.09±0.04	0.41	1
77)	NDWFS J143232.5+351534	14:32:32.484	35:15:34.23	35.3	GROUP	23.45±0.07	0.30	1
78)	NDWFS J143651.3+342107	14:36:51.312	34:21:07.38	35.1	GROUP	23.71±0.05	0.28	1
79)	NDWFS J142746.3+344544	14:27:46.348	34:45:44.02	35.0	GROUP	23.39±0.04	0.34	1
80)	NDWFS J142548.3+322957	14:25:48.283	32:29:56.58	35.0	GROUP	23.83±0.06	0.12	1
81)	NDWFS J142735.5+342332	14:27:35.479	34:23:32.38	35.0	GROUP	23.55±0.04	-0.26	1
82)	NDWFS J142449.8+324743	14:24:49.761	32:47:42.61	34.9	GROUP	24.09±0.09	-0.74	1
83)	NDWFS J142732.5+341213	14:27:32.520	34:12:13.39	34.4	GROUP	23.62±0.05	-0.62	1
84)	NDWFS J142802.8+350933	14:28:02.803	35:09:33.30	34.2	GROUP	23.80±0.06	0.35	1
85)	NDWFS J142533.0+343912	14:25:32.966	34:39:11.95	28.8	DIFFUSE	23.67±0.06	0.26	3

^a Morphological flag discussed in Section 2.2.6: GROUP - tight grouping of compact sources, DIFFUSE - spatially-extended diffuse emission.

^b Magnitudes and colors were measured using large 30 pix (7.7'') diameter apertures.

^c Priority assignments are discussed in Section 2.2.7.

^d The two largest candidates are in fact part of a single diffuse, asymmetric, and mostly linear structure. The unusual morphology and large size suggest that this is more likely some sort of Galactic nebula rather than an extragalactic source. The optical spectrum (Paper II) does not show any obvious emission features, suggesting that this might be a reflection nebula.

^e Our search recovered LABd05, the Ly α nebula found previously by Dey et al. (2005). The listed coordinates are those returned by the search algorithm.

^f Our search discovered PRG1, a Ly α nebula at $z \approx 1.67$ (Prescott et al. 2009, Paper II).

^g Our search discovered PRG2, a Ly α nebula at $z \approx 2.27$ (Prescott 2009, Paper II).

^h Our search discovered PRG3, a Ly α nebula at $z \approx 2.14$ (Prescott 2009, Paper II).

ⁱ Our search discovered PRG4, a Ly α nebula at $z \approx 1.88$ (Prescott 2009, Paper II).

Table 2
Wide-Area Ly α Nebula Surveys

Survey	Field ^a	Redshift	Δz	Area (deg ²)	Comoving Volume (10 ⁶ h ₇₀ ⁻³ Mpc ³)
Matsuda et al. 2004	SSA22	3.09	0.06	0.20	0.14
Palunas et al. 2004	J2143-4423	2.38	0.04	0.56	0.30
Saito et al. 2006	SXDS	3.34	0.20	0.23	0.53
	SXDS	3.72	0.22	0.23	0.56
	SXDS	3.93	0.24	0.23	0.60
	SXDS	4.12	0.24	0.23	0.59
	SXDS	4.35	0.26	0.23	0.62
	SXDS	4.58	0.28	0.23	0.65
	SXDS	4.82	0.26	0.23	0.59
Smith & Jarvis 2007	XMM-LSS, LH, SFLS	2.85	0.08	≈15 ^b	≈14.7
	XMM-LSS, LH, SFLS	3.00	0.14	≈15 ^b	≈24.8
	XMM-LSS, LH, SFLS	3.12	0.08	≈15 ^b	≈14.5
Matsuda et al. 2009	B3J2330+3927	3.09	0.06	0.25	0.18
Ouchi et al. 2009	SXDS	6.56	0.10	1.00	0.82
Yang et al. 2009	NDWFS Boötes	2.30	0.04	4.82	2.14
Yang et al. 2010	CDF-N	2.30	0.04	0.28	0.12
	CDF-S	2.30	0.04	0.24	0.11
	COSMOS1	2.30	0.04	0.36	0.16
	COSMOS2	2.30	0.04	0.36	0.16
Matsuda et al. 2011	SSA22	3.09	0.06	1.06	0.74
	SXDS	3.09	0.06	0.60	0.42
	GOODS-N	3.09	0.06	0.24	0.17
	SDF	3.09	0.06	0.22	0.16
This work	NDWFS Boötes	1.6-2.9	1.3	8.5	130

^a Abbreviated field names correspond to the following: COSMOS1 & COSMOS2 - two pointings within the Cosmic Evolution Survey (COSMOS) field, CDF-N - Chandra Deep Field North, CDF-S - Chandra Deep Field South, B3J2330+3927 - a high redshift radio galaxy field, GOODS-N - Great Observatories Origins Deep Survey North field, J2143-4423 - a galaxy cluster field, LH - Lockman Hole field, NDWFS Boötes - NOAO Deep Wide-Field Survey Boötes field, SDF - Subaru Deep Field, SFLS - Spitzer First Look Survey field, SSA22 - Small Selected Area 22 field originally from Lilly et al. (1991), SXDS - Subaru/XMM-Newton Deep Survey, XMM-LSS - XMM-Newton Large Scale Structure Survey field.

^b Exact survey area was not given in Smith & Jarvis (2007).

Table 3
Known Ly α Nebulae in the NDWFS Boötes Field

Source	Survey ^a	Redshift	B_W Isophotal Area ^b (arcsec ²)	B_W Surface Brightness ^c (mag arcsec ⁻²)	Notes ^d
LABd05	Dey et al. (2005)	2.7	54.4	27.0	Recovered
P1	Prescott et al. - Subaru	2.7	27.6	27.3	Too Faint
P2	Prescott et al. - Subaru	2.6	71.0	26.9	Core-Halo
P3	Prescott et al. - Mayall	1.9	25.4	26.9	Core-Halo
Y1	Yang et al. (2009)	2.3	20.4	26.7	Core-Halo
Y2	Yang et al. (2009)	2.3	17.0	26.8	Core-Halo
Y3	Yang et al. (2009)	2.3	36.6	25.9	Core-Halo
Y4	Yang et al. (2009)	2.3	37.5	26.6	Core-Halo

^a Spectroscopically confirmed Ly α nebulae selected from a Subaru intermediate-band survey (Prescott et al. 2012, in preparation) and a Mayall intermediate-band survey (Prescott et al. 2012, in preparation) are listed along with Ly α nebulae from the narrow-band survey by Yang et al. (2009).

^b Isophotal area determined using SourceExtractor and a detection threshold set to the median 1σ surface brightness threshold of the NDWFS B_W imaging (Section 4.2).

^c Mean surface brightness within the isophotal area determined using SourceExtractor (Section 4.2).

^d “Too Faint” indicates that the diffuse emission was too faint to be selected by our survey. “Core-Halo” describes sources with a central compact continuum source surrounded by a Ly α halo; these sources are partially or completely removed from the images during pipeline steps designed to remove bright stars and compact galaxies and are not selected by our survey.

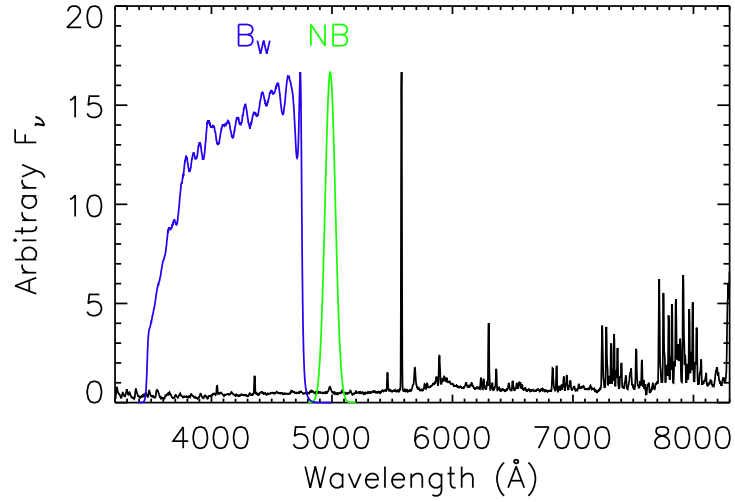


Figure 1. Broad-band B_W bandpass and a generic narrow-band filter bandpass (NB; FWHM = 100\AA) overlaid on a spectrum of the night sky. Our systematic broad-band search technique, designed to find luminous Ly α nebulae at $2 \lesssim z \lesssim 3$, is able to efficiently survey enormous comoving volumes by relying on deep, wide-field, broad-band imaging and the very dark sky in the blue.

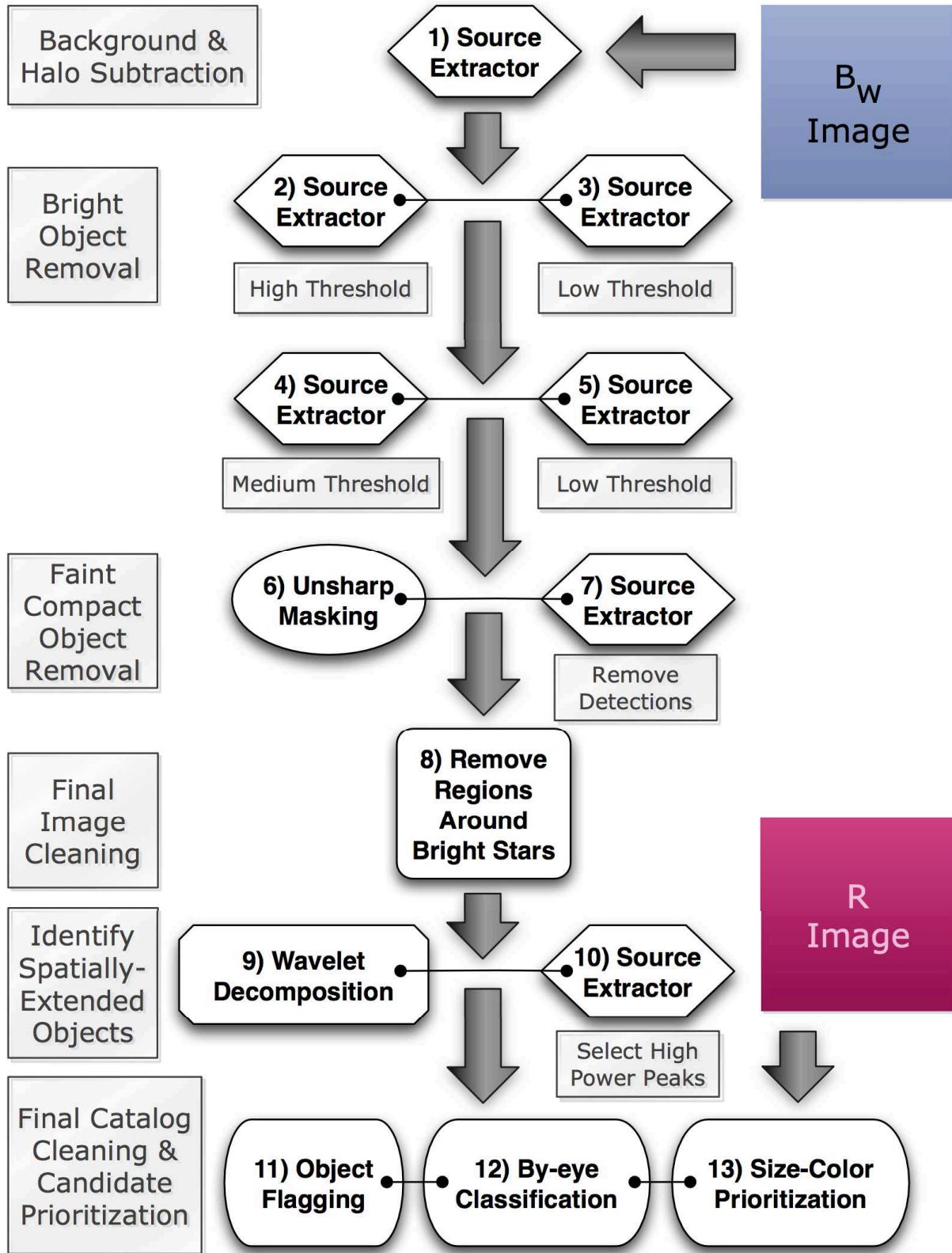


Figure 2. Flowchart outlining the individual steps of our systematic broad-band search for luminous Ly α nebulae.

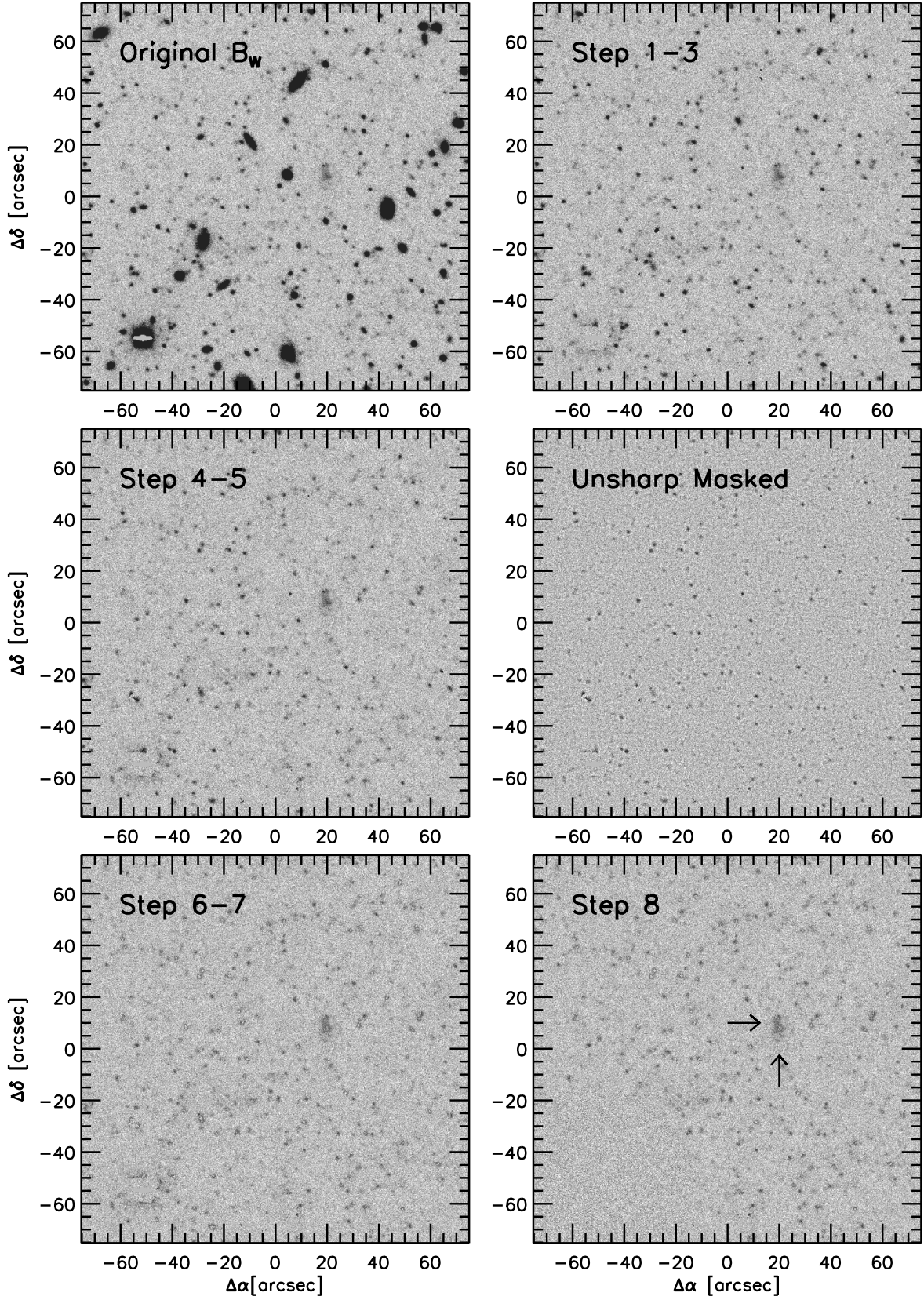


Figure 3. Individual steps of the broad-band Ly α nebula search algorithm illustrated using the region around LABd05 (Section 2.2). The diffuse emission of LABd05 is clearly visible (arrows) in the final frame (*Step 8*).

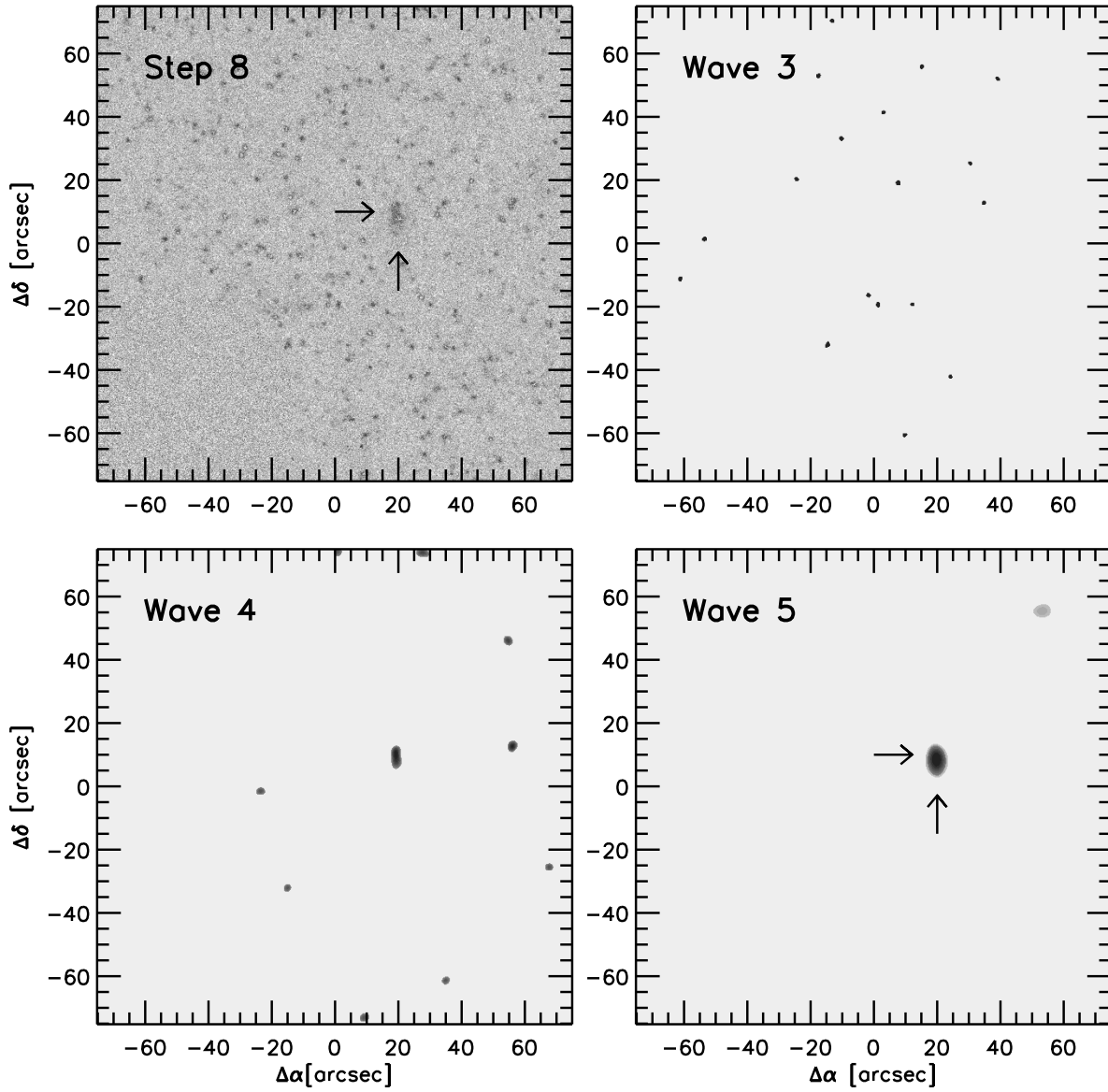


Figure 4. Wavelet decomposition is used to separate out sources of different size scales. The upper left panel shows the final result of Steps 1-8 of the search algorithm, as in Figure 3. The other three panels show the wavelet power maps for different size scales. The diffuse emission of LABd05 generates a large wavelet power peak in the final panel and is easily selected as a Ly α nebula candidate (arrows). The source in the upper righthand corner of the final panel was below the 4σ threshold (Section 2.2.5) and was not selected.

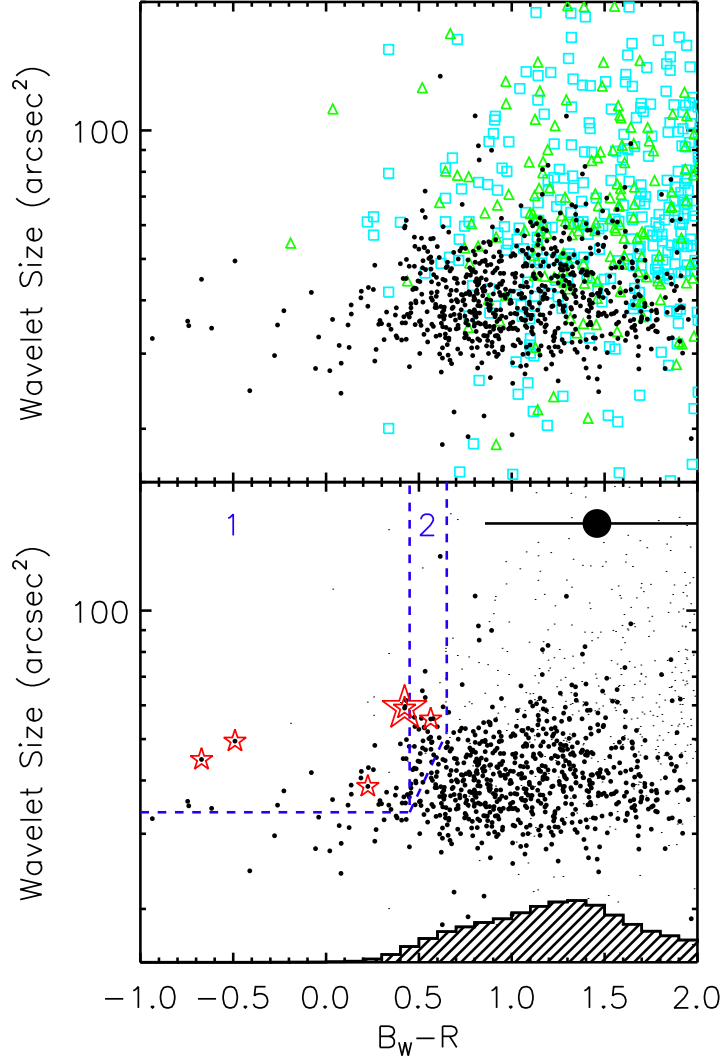


Figure 5. Wavelet Size vs. $B_W - R$ color for Ly α nebula candidates selected using the morphological search pipeline. The wavelet size corresponds to the size of the source in the wavelet power map, but does not indicate the true nebular size of the object (Section 2.2.7). **Top:** Ly α nebula candidates are shown (black circles) along with artifacts from the residual halos of bright galaxies (GALAXY; cyan squares) and detections of tidal tails and spiral arms (TIDAL/ARM; green triangles). **Bottom:** Ly α nebula candidates are shown as in the top panel (black circles), with first and second priority selection regions indicated (blue dashed lines). The first (second) priority region contains 39 (40) Ly α nebula candidates. LABd05 is indicated with a double star (Dey et al. 2005), and the other spectroscopically-confirmed Ly α nebulae are shown as single stars (Prescott et al. 2009, Paper II). Artifacts from the upper panel are indicated with small black dots. The large filled black circle with an error bar represents the typical color of low surface brightness galaxies (LSBs; Habertz et al. 2007), and the histogram (plotted on a linear scale) represents the distribution of $B_W - R$ colors for field galaxies in NDWFS, demonstrating that the colors of our final Ly α nebula candidates are substantially bluer than typical LSBs and field galaxies.

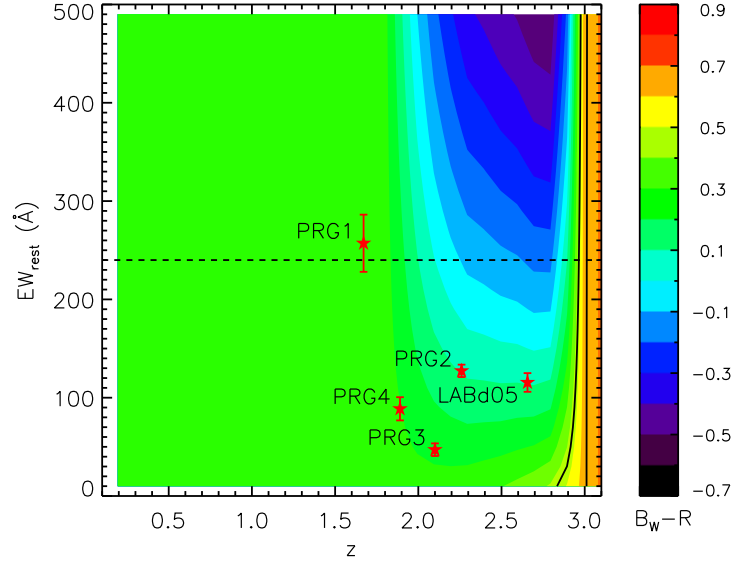


Figure 6. Expected $B_W - R$ colors for $\text{Ly}\alpha$ nebulae at redshifts $0.1 < z < 3.1$, where the colors are divided into 0.1 mag bins; the $B_W - R$ color cuts used in our survey are shown as black lines at $B_W - R < 0.45$ and at $B_W - R < 0.65$. $\text{Ly}\alpha$ nebulae are modeled as flat spectrum sources ($f_\lambda \propto \lambda^{-2}$) with $\text{Ly}\alpha$ emission lines of varying equivalent widths, where the continuum at the position of $\text{Ly}\alpha$ is measured using a 20\AA bin redward of the line. The B_W bandpass contains $\text{Ly}\alpha$ at $1.9 \lesssim z \lesssim 2.9$, leading to blue colors. However, due to the wavelength range of the spectroscopic follow-up observations, $\text{Ly}\alpha$ nebulae can be detected as spatially extended sources even at lower redshifts ($z \gtrsim 1.6$) if the continuum has the same extended morphology as the $\text{Ly}\alpha$, even though $\text{Ly}\alpha$ is not contained with the B_W band. The canonical upper limit for $\text{Ly}\alpha$ equivalent widths arising from stellar processes is shown (240\AA , dashed line; Charlot & Fall 1993) along with the positions in redshift- EW_{rest} space of the confirmed $\text{Ly}\alpha$ nebulae (Dey et al. 2005; Prescott et al. 2009, Paper II). The $B_W - R$ colors of actual $\text{Ly}\alpha$ nebulae can and do deviate from the colors predicted using this simple model most likely due to, e.g., differing continuum shapes, the composite nature of actual $\text{Ly}\alpha$ nebula systems, the presence of embedded sources with different colors.

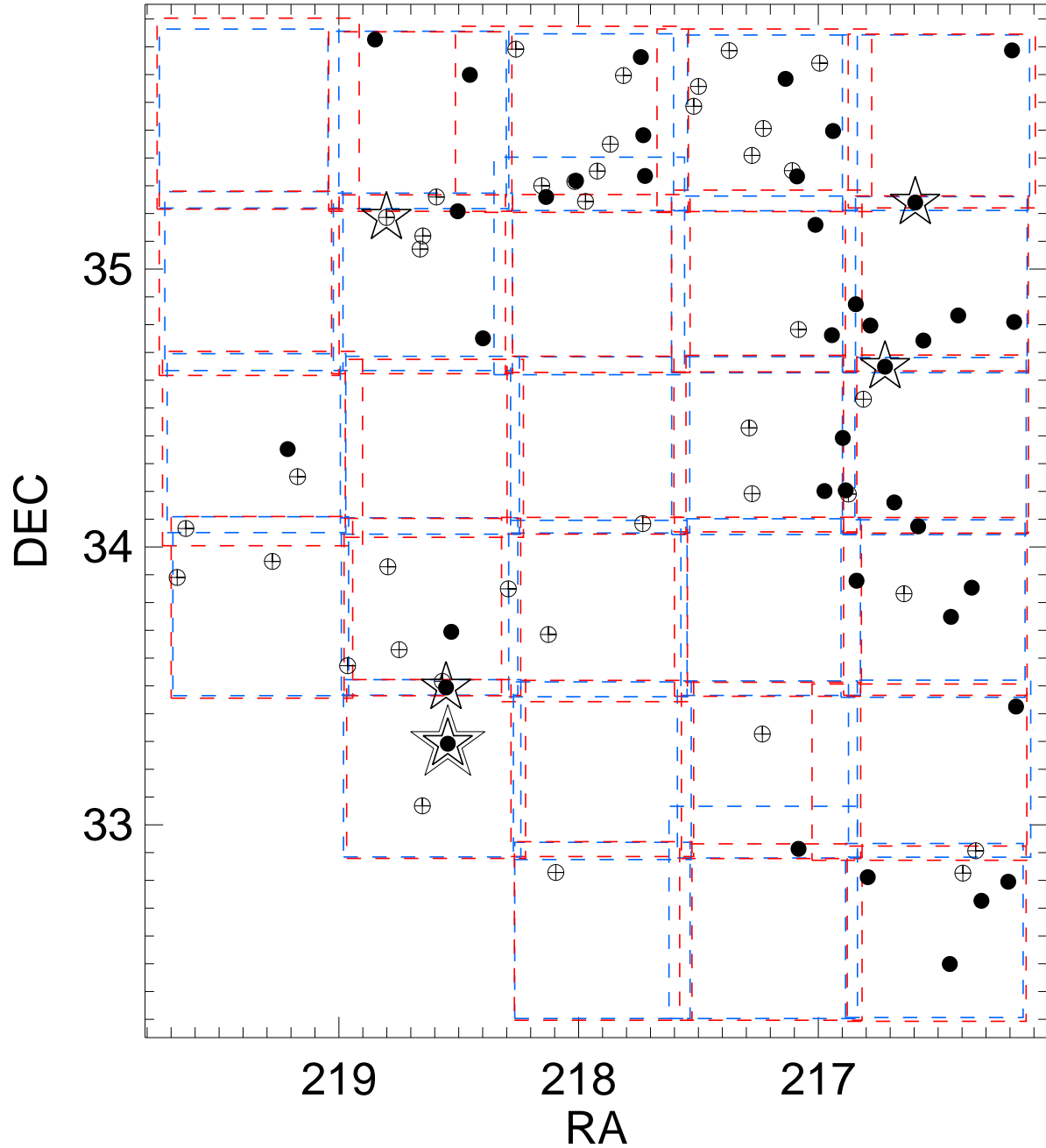


Figure 7. Sky distribution of priority 1 (filled circles) and priority 2 (crossed open circles) Ly α nebula candidates within the NDWFS Boötes field. The individual NDWFS tiles are shown as blue (B_W imaging) and red (R -band imaging) dashed rectangles. Confirmed Ly α nebulae are shown as stars (Paper II), including LABd05 (double star; Dey et al. 2005).

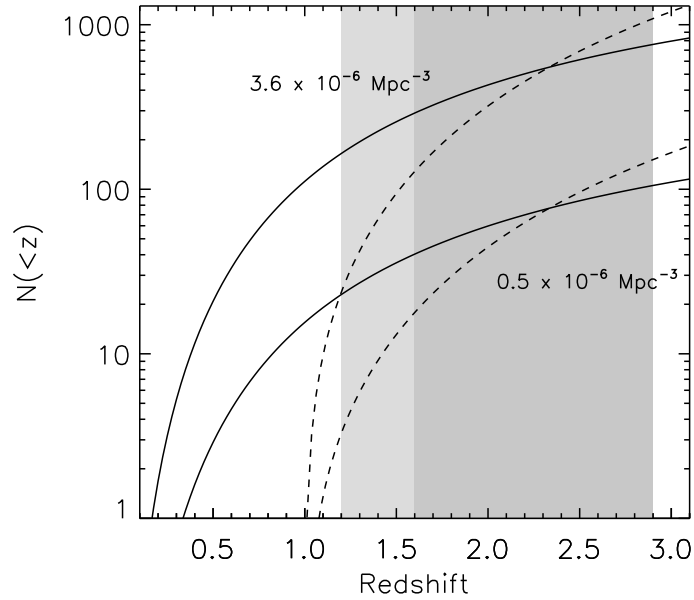


Figure 8. Cumulative expected number of Ly α nebulae assuming a constant (i.e., redshift independent) comoving volume density of $0.5 \times 10^{-6} - 3.6 \times 10^{-6} \text{ Mpc}^{-3}$ (the range estimated for $z \approx 2.3$ by Yang et al. 2009) as a function of redshift and a 100% detection rate (solid lines). The dashed lines show the cumulative expected number of Ly α nebulae under the assumption that the comoving volume density increases linearly to higher redshift and matches the measured rate at $z = 2.3$. Our survey is designed to select Ly α nebulae at redshifts $z \approx 1.6 - 2.9$ (dark grey shading); however, Ly α nebulae at $z \approx 1.2 - 1.6$ (light grey shading) with diffuse blue continuum emission that are selected by our morphological survey will appear as continuum-only sources in follow-up spectroscopy.

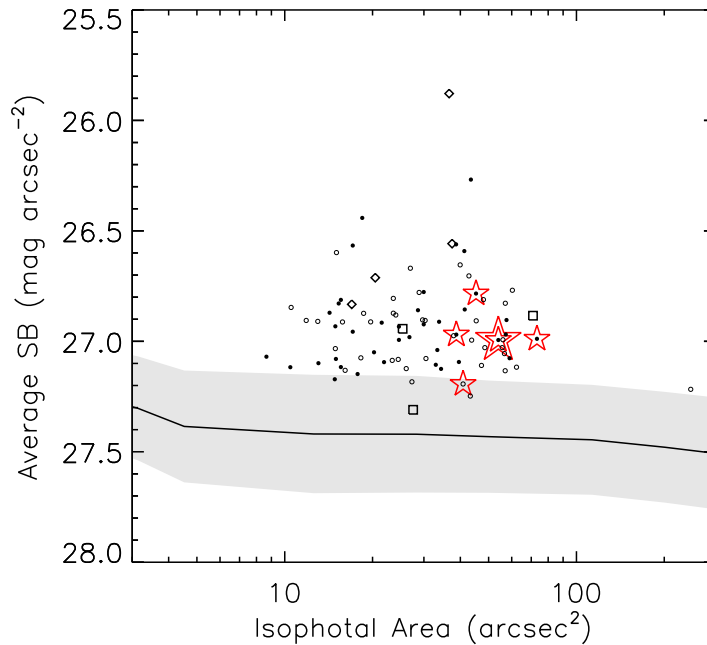


Figure 9. Average surface brightness versus isophotal area (above the median surface brightness limit of the NDWFS survey; $28.9 \text{ mag arcsec}^{-2}$, 1σ , $1.1''$ diameter aperture) for both first (filled circles) and second (open circles) priority candidates. Confirmed Ly α nebulae from this survey are indicated with stars (Paper II), including LABd05 (double star; Dey et al. 2005). Spectroscopically confirmed Ly α sources in the Boötes field from other surveys that were not selected by our broad-band search (Table 3), primarily due to the presence of bright central sources, are shown as diamonds (Yang et al. 2009) and squares (Prescott et al. 2012e, in prep.). The median 5σ surface brightness limit of the survey is shown as the black line, with the standard deviation of all 27 pointings shown as a shaded band.

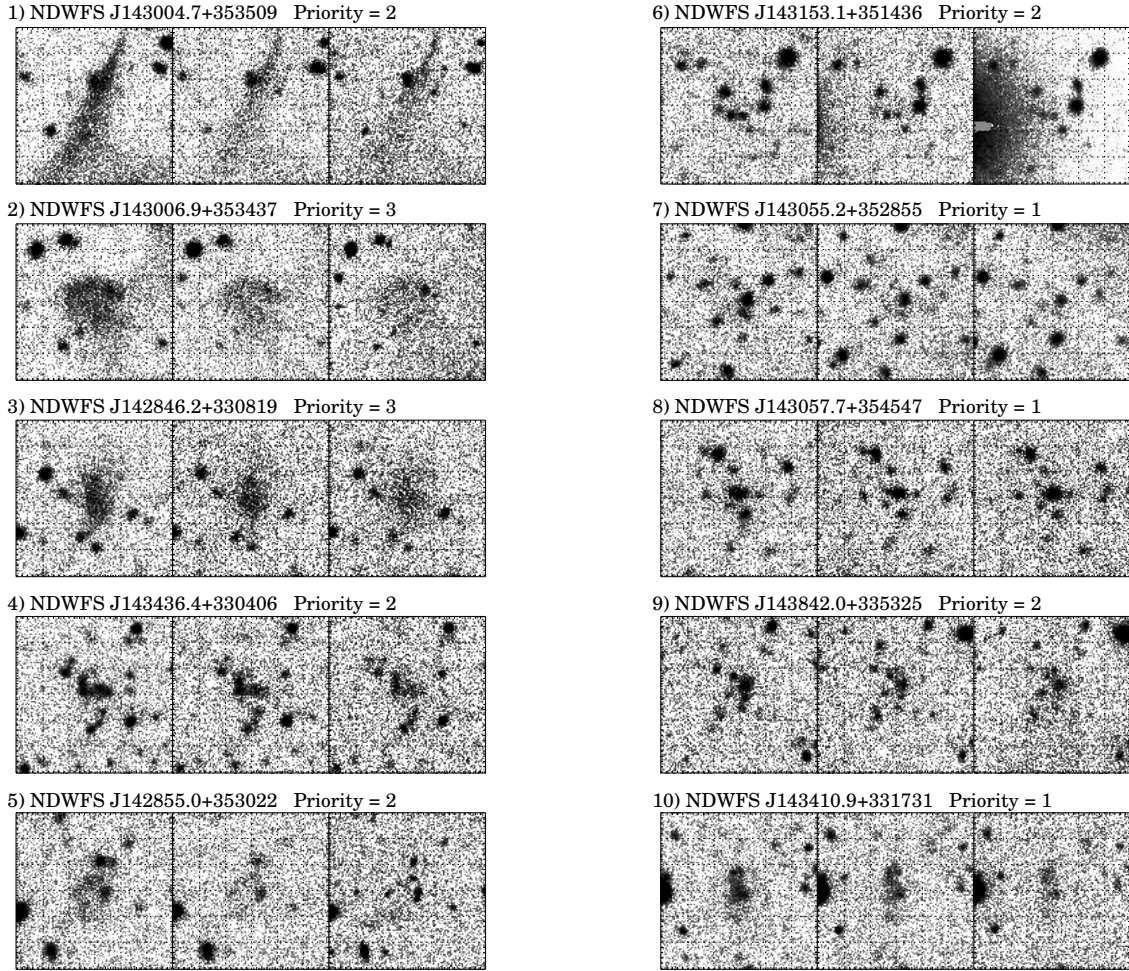


Figure 10. Postage stamp images of the Ly α nebula candidates in the B_W , R , and I bands, respectively. Images are displayed using a log scaling within $30'' \times 30''$ boxes, and are labeled with the candidate number, name, and priority listed in Table 1.

APPENDIX POSTAGE STAMPS

Postage stamp images of the 79 Ly α nebula candidates from our broad-band survey of the NDWFS Boötes field. The B_W and R -band images shown were used for morphological and color selection during the survey; the I -band images are shown for reference.

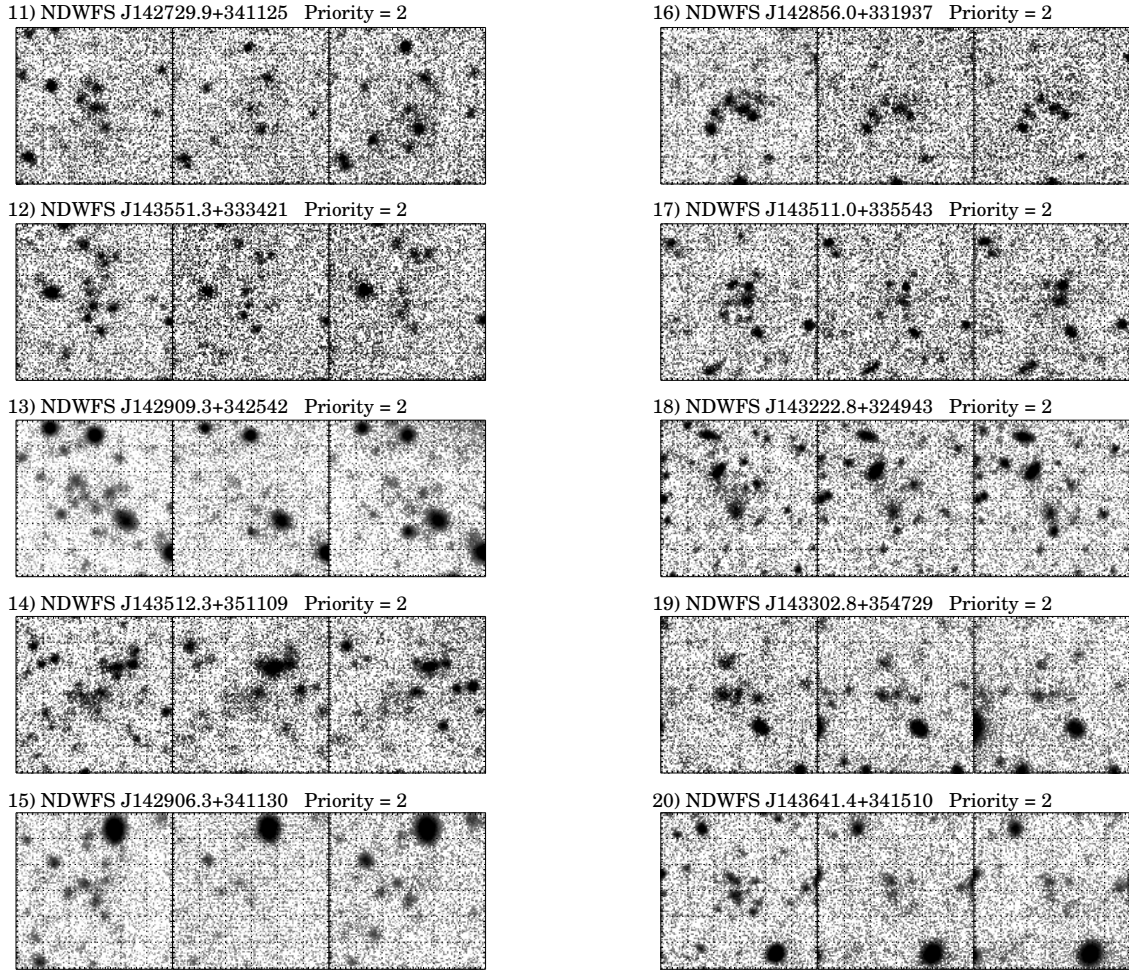


Figure 11. Postage stamp images of the Ly α nebula candidates in the B_W , R , and I bands, respectively. Images are displayed using a log scaling within $30'' \times 30''$ boxes, and are labeled with the candidate number, name, and priority listed in Table 1.

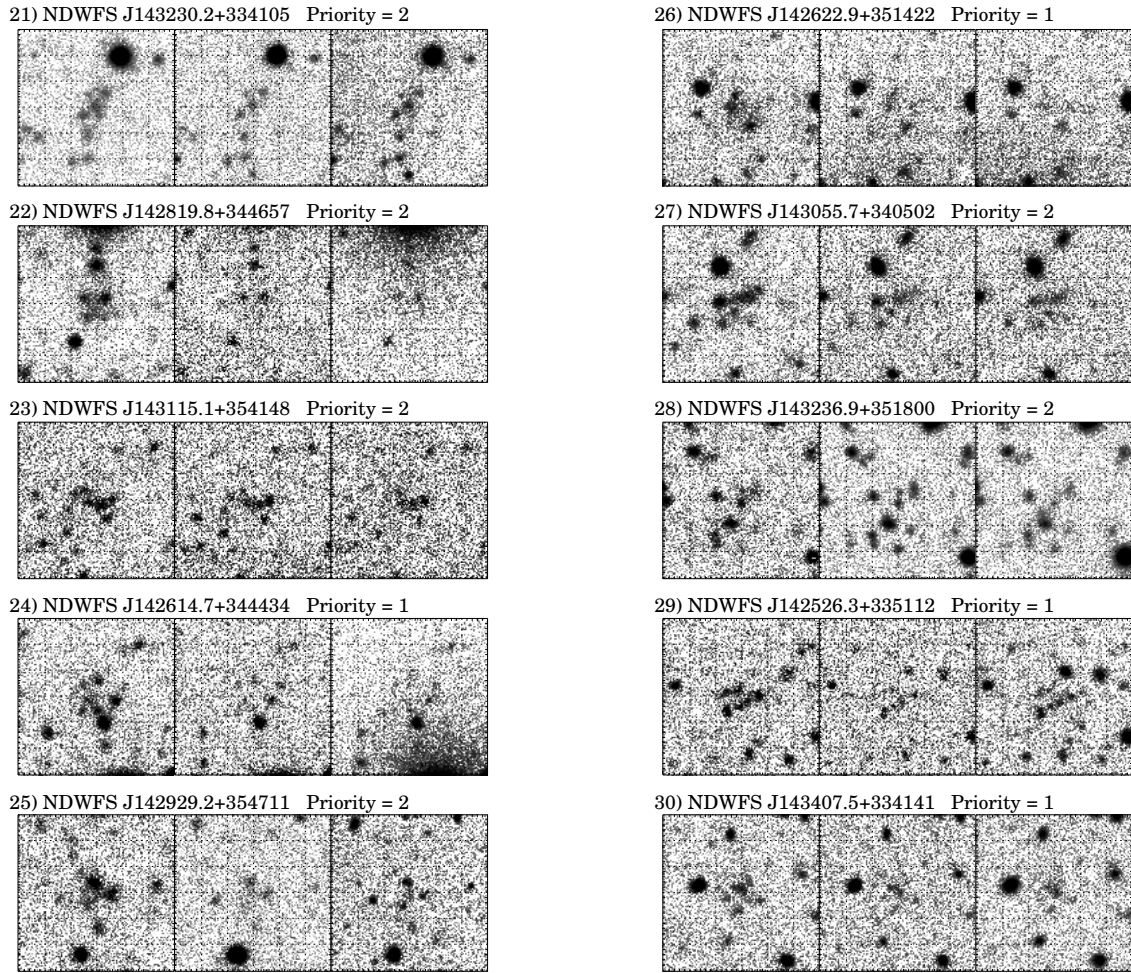


Figure 12. Postage stamp images of the Ly α nebula candidates in the B_W , R , and I bands, respectively. Images are displayed using a log scaling within $30'' \times 30''$ boxes, and are labeled with the candidate number, name, and priority listed in Table 1.

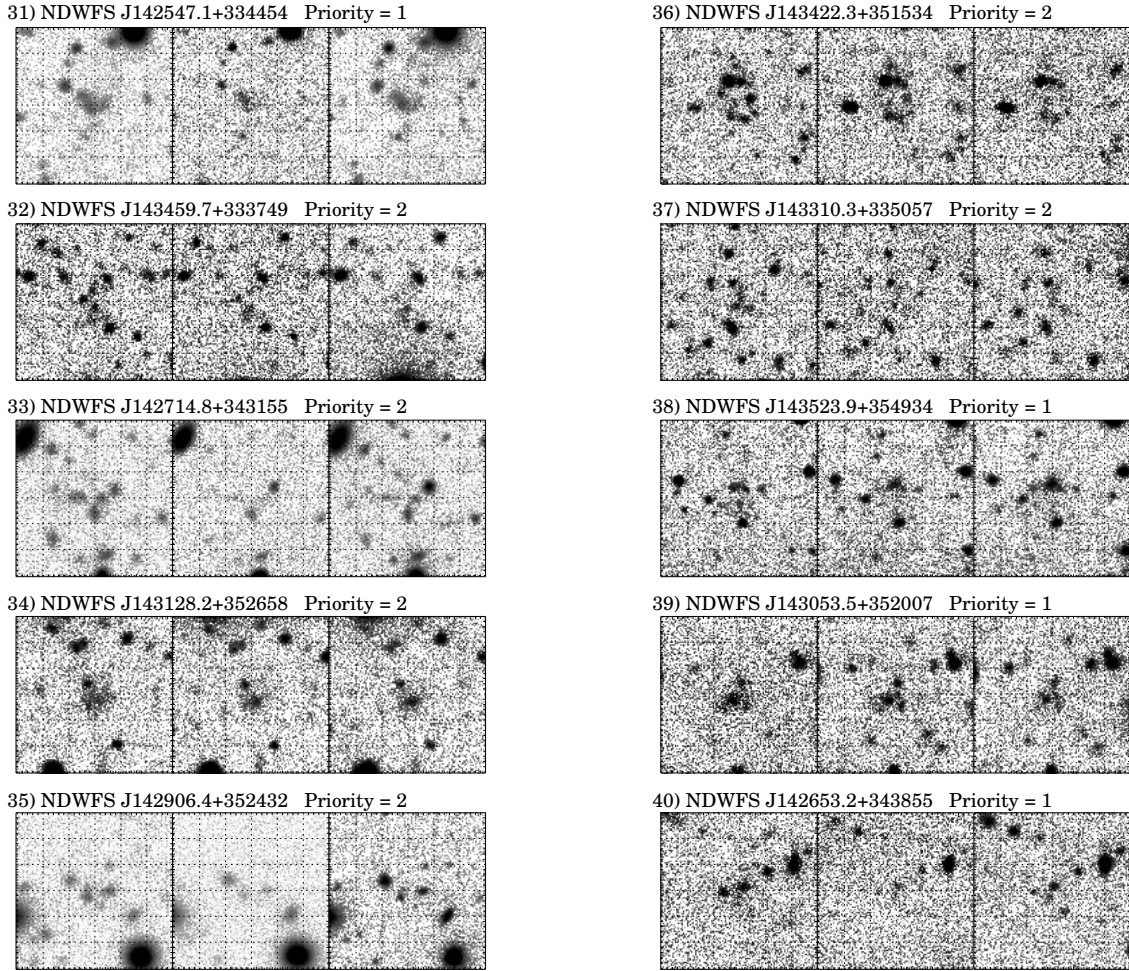


Figure 13. Postage stamp images of the Ly α nebula candidates in the B_W , R , and I bands, respectively. Images are displayed using a log scaling within $30'' \times 30''$ boxes, and are labeled with the candidate number, name, and priority listed in Table 1.

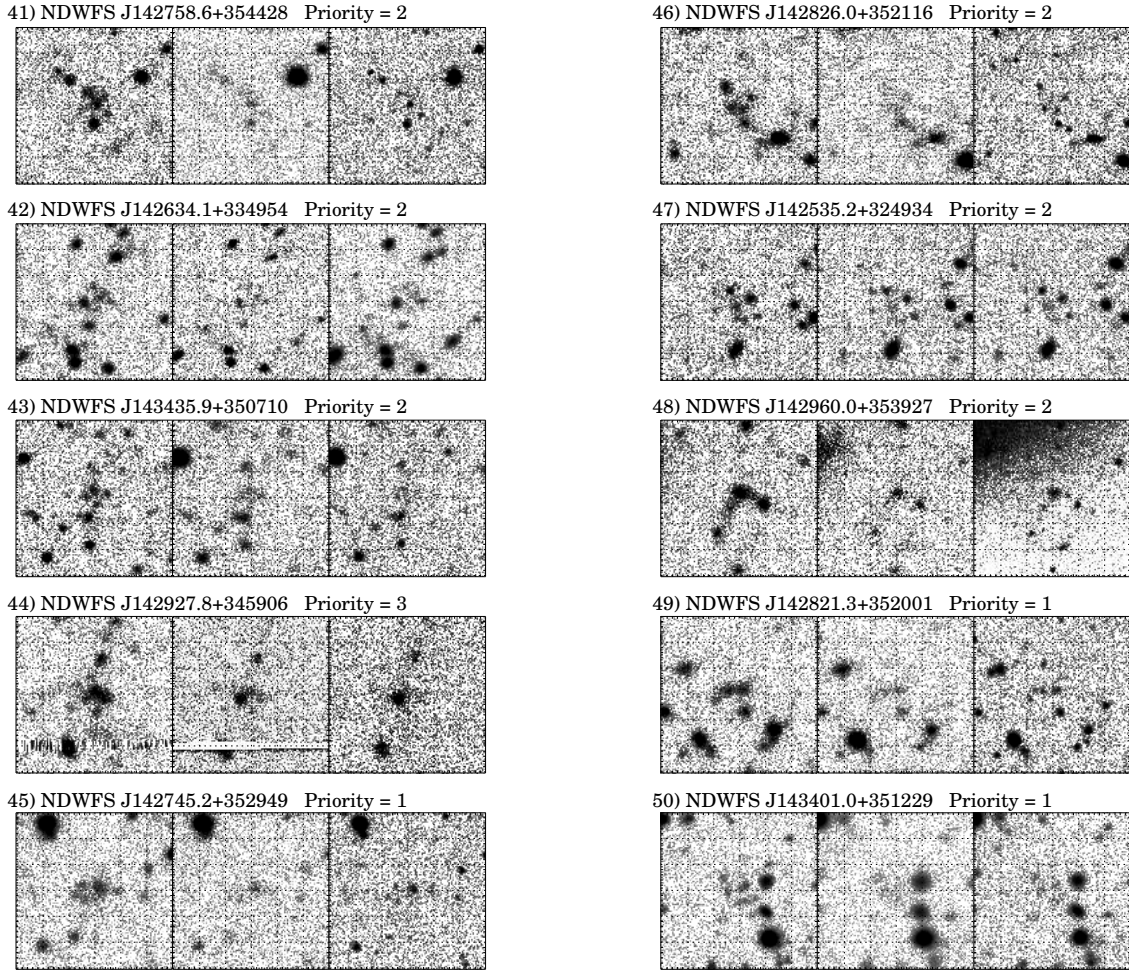


Figure 14. Postage stamp images of the Ly α nebula candidates in the B_W , R , and I bands, respectively. Images are displayed using a log scaling within $30'' \times 30''$ boxes, and are labeled with the candidate number, name, and priority listed in Table 1.

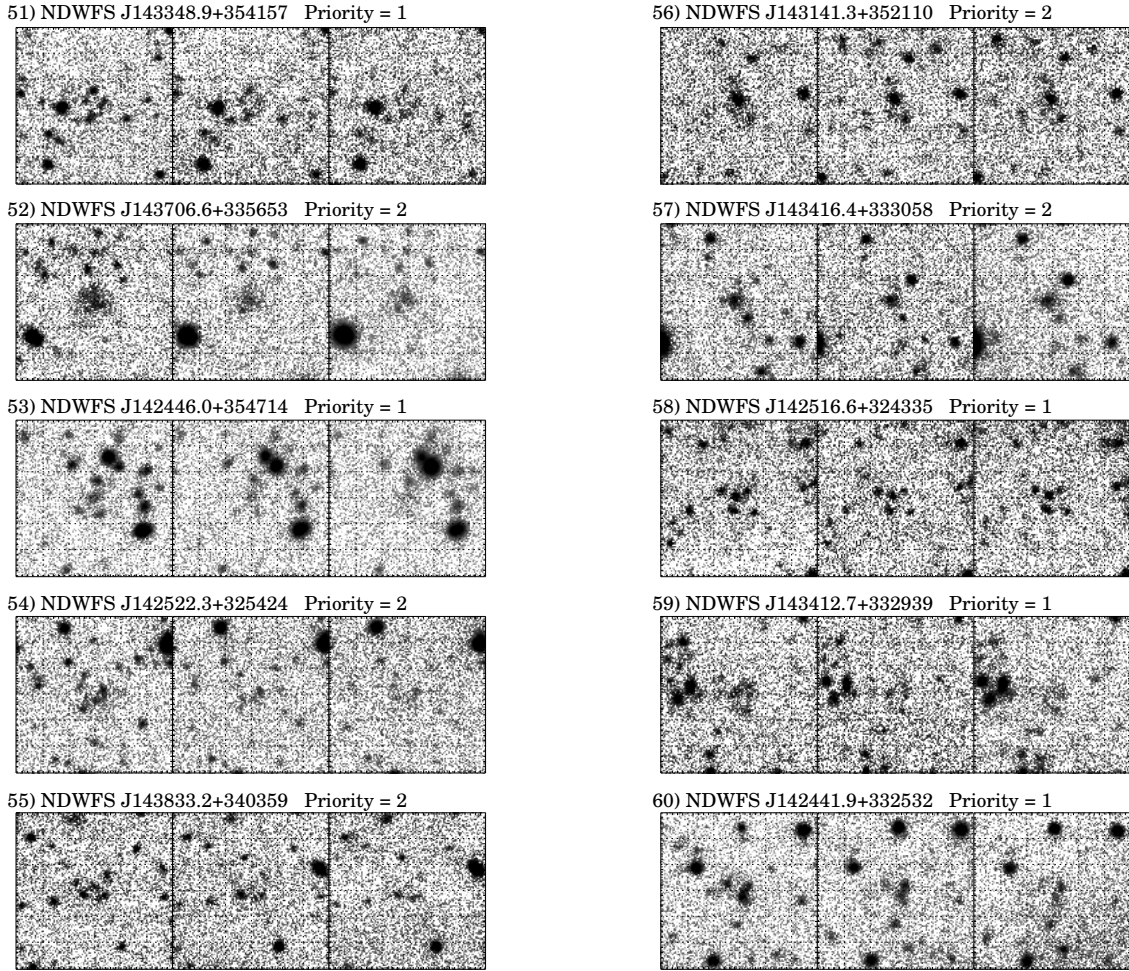


Figure 15. Postage stamp images of the Ly α nebula candidates in the B_W , R , and I bands, respectively. Images are displayed using a log scaling within $30'' \times 30''$ boxes, and are labeled with the candidate number, name, and priority listed in Table 1.

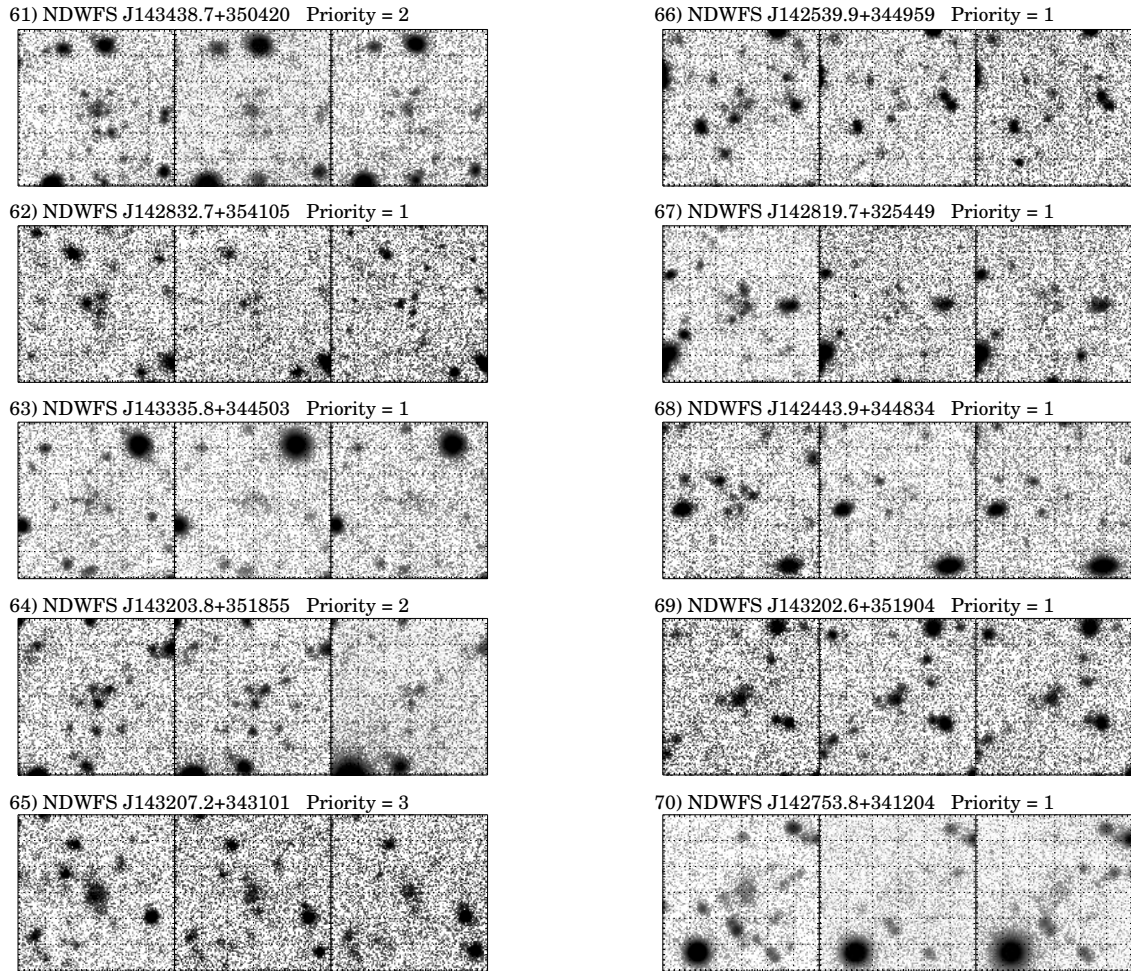


Figure 16. Postage stamp images of the Ly α nebula candidates in the B_W , R , and I bands, respectively. Images are displayed using a log scaling within $30'' \times 30''$ boxes, and are labeled with the candidate number, name, and priority listed in Table 1.

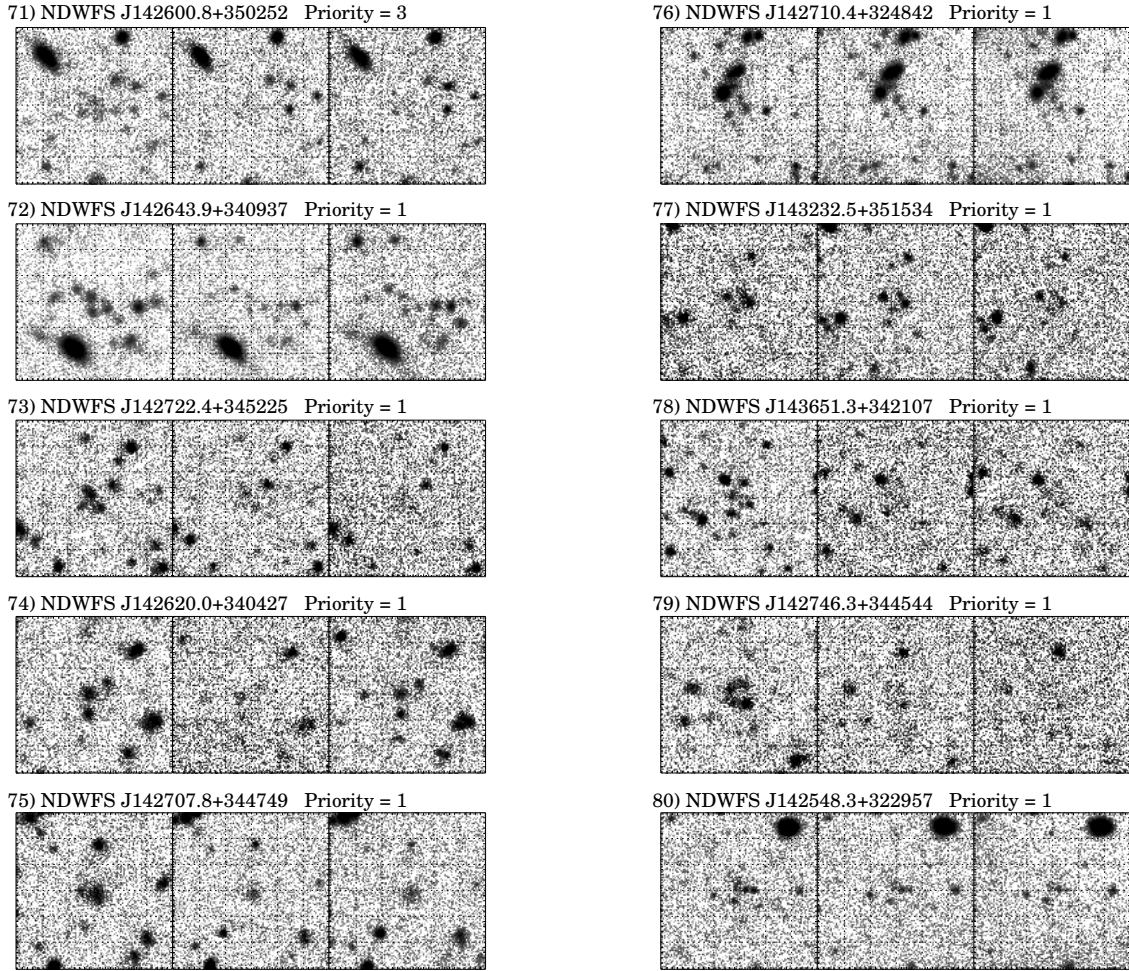
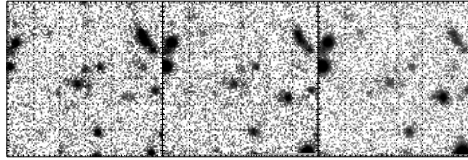


Figure 17. Postage stamp images of the Ly α nebula candidates in the B_W , R , and I bands, respectively. Images are displayed using a log scaling within $30'' \times 30''$ boxes, and are labeled with the candidate number, name, and priority listed in Table 1.

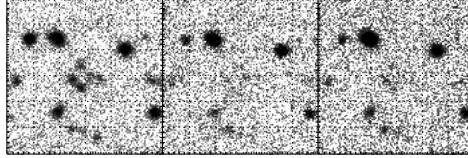
81) NDWFS J142735.5+342332 Priority = 1



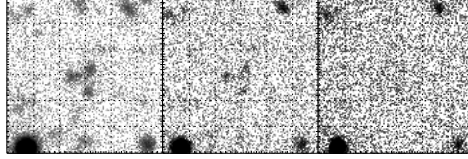
82) NDWFS J142449.8+324743 Priority = 1



83) NDWFS J142732.5+341213 Priority = 1



84) NDWFS J142802.8+350933 Priority = 1



85) NDWFS J142533.0+343912 Priority = 3

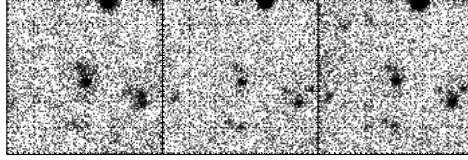


Figure 18. Postage stamp images of the Ly α nebula candidates in the B_W , R , and I bands, respectively. Images are displayed using a log scaling within $30'' \times 30''$ boxes, and are labeled with the candidate number, name, and priority listed in Table 1.